Published in final edited form as:
J Med Chem. 2017 May 11; 60(9): 3814–3827. doi:10.1021/acs.jmedchem.7b00018.

Second Generation Triple-Helical Peptide Inhibitors of Matrix Metalloproteinases

Manishabrata Bhowmick[†,‡,○], **Dorota Tokmina-Roszyk**[§,◆], **Lillian Onwuha-Ekpete**[§,¶], **Kelli Harmon**[‖,×], **Trista Robichaud**[⊥,+], **Rita Fuerst**[#,∞], **Roma Stawikowska**[§,£], **Bjorn Steffensen**[⊥,∇,△], **William Roush**[#,◇,iD], **Hector R. Wong**[‖,∀], and **Gregg B. Fields**[*,§,#,iD]

[†]Torrey Pines Institute for Molecular Studies, 11350 SW Village Parkway, Port St. Lucie, Florida 34987, United States

[‡]Sigma-Aldrich Corporation, 3 Strathmore Road, Natick, Massachusetts 01760, United States

[§]Florida Atlantic University, 5353 Parkside Drive, Jupiter, Florida 33458, United States

[‖]Cincinnati Children's Hospital Medical Center, 3333 Burnet Avenue, Cincinnati, Ohio 45229, United States

[⊥]University of Texas Health Science Center, 7703 Floyd Curl Drive, San Antonio Texas 78229, United States

[#]The Scripps Research Institute/Scripps Florida, 130 Scripps Way, Jupiter, Florida 33458, United States

[∇]School of Dental Medicine, Tufts University, 1 Kneeland Street, Boston, Massachusetts 02111, United States

Abstract

The design of selective matrix metalloproteinase (MMP) inhibitors that also possess favorable solubility properties has proved to be especially challenging. A prior approach using collagen-model templates combined with transition state analogs produced a first generation of triple-helical peptide inhibitors (THPIs) that were effective in vitro against discrete members of the

[iD]**ORCID**
William Roush: 0000-0001-9785-5897
Gregg B. Fields: 0000-0003-3573-1527
[○]M.B.: manishabrata.bhowmick@sial.com.
[◆]D.T.-R.: dtokminarosz2013@fau.edu.
[¶]L.O.-E.: lonwuhae@fau.edu.
[×]K.H.: Kelli.Odoms@cchmc.org.
[+]T.R.: trista.k.robichaud@lonestar.edu.
[∞]R.F.: rfuerst@scripps.edu.
[£]R.S.: rstawikowska@fau.edu.
[△]B.S.: bjorn.steffensen@tufts.edu.
[◇]W.R.: roush@scripps.edu.
[∀]H.R.W.: hector.wong@cchmc.org.
[*]**Corresponding Author**: Phone: +1-561-799-8577. fieldsg@fau.edu, gfields@scripps.edu.
The authors declare no competing financial interest.

Europe PMC Funders Author Manuscripts

MMP family. These THPI constructs were also highly water-soluble. The present study sought improvements in the first generation THPIs by enhancing thermal stability and selectivity. A THPI selective for MMP-2 and MMP-9 was redesigned to incorporate non-native amino acids (Flp and mep), resulting in an increase of 18 °C in thermal stability. This THPI was effective in vivo in a mouse model of multiple sclerosis, reducing clinical severity and weight loss. Two other THPIs were developed to be more selective within the collagenolytic members of the MMP family. One of these THPIs was serendipitously more effective against MMP-8 than MT1-MMP and was utilized successfully in a mouse model of sepsis. The THPI targeting MMP-8 minimized lung damage, increased production of the anti-inflammatory cytokine IL-10, and vastly improved mouse survival.

Introduction

Collagenolysis is a well-known physiological process involved in normal tissue and organ development, morphogenesis, and wound healing.1 Conversely, pathological conditions resulting from abnormal collagen catabolism include primary and metastatic tumor growth, arthritis, arteriosclerosis, and periodontitis.1–4 The matrix metalloproteinases (MMPs) are the most extensively studied proteases that catalyze the hydrolysis of the collagen triple-helix.5

MMP inhibitor programs began in the early 1980s, using extracellular matrix substrates as models for inhibitor design.6 The first generation of MMP inhibitors were peptidic whereas the second generation were nonpeptidic small molecules.2,7 However, clinical trials with both generations of MMP inhibitors were unsuccessful due to, among several reasons, a lack of inhibitor selectivity and metabolic stability, suboptimal dosing of inhibitor, and often considerable side effects.2,8–11

A well-established strategy to develop protease inhibitors is modification of a bioactive peptide such that the hydrolytically susceptible peptide bond is replaced. The use of phosphinic pseudo-dipeptides can be a very effective approach to develop highly selective and potent inhibitors of a variety of Zn^{2+} metalloproteases.12,13 Phosphinic dipeptides contain a hydrolytically stable, tetrahedral phosphinic moiety that mimics the tetrahedral intermediate formed during enzymatic hydrolysis. Previously, we reported that phosphinic triple-helical peptides (THPs) behave as effective transition state analog inhibitors of collagenolytic MMPs.12,14,15 More specifically, two homotrimeric triple-helical peptide inhibitors (THPIs), C_6-(Gly-Pro-Hyp)$_4$-Gly-Pro-Pro-GlyΨ{PO_2H-CH_2}Val-Val-Gly-Glu-Gln-Gly-Glu-Gln-Gly-Pro-Pro-(Gly-Pro-Hyp)$_4$-NH_2 [designated C_6-α1(V)GlyΨ{PO_2H-CH_2}Val THPI] and (Gly-Pro-Hyp)$_4$-Gly-mep-Flp-Gly-Pro-Gln-GlyΨ{PO_2H-CH_2}Leu-Ala-Gly-Gln-Arg-Gly-Ile-Arg-Gly-mep-Flp-(Gly-Pro-Hyp)$_4$-Tyr-NH_2 [designated α1(I-III)GlyΨ{PO_2H-CH_2}Leu THPI], were shown to inhibit MMPs in the low nanomolar range.12,14 The THPI sequences were based on either the α1(V)436−450 collagen region, which is hydrolyzed at the Gly-Val bond by MMP-2 and MMP-9, or the interstitial collagen consensus sequence α1(I−III)769−783, which is hydrolyzed by MMP-1, MMP-2, MMP-8, MMP-9, MMP-13, membrane-type 1 MMP (MT1-MMP), and MT2-MMP.16,17

THPIs represent small, well-folded peptidic structures. There has been a recent surge in the advancement of peptide drugs, as they tend to have lower toxicities and greater efficacies than existing drugs.18–21 The size of THPIs makes immunogenicity unlikely; in fact, with the exclusion of specific glycosylated sequences, collagen peptides are nonimmunogenic. The triple-helical nature of the inhibitor renders it reasonably stable to proteolysis, as observed in vitro in mouse, rat, and human serum and/or plasma and in vivo in rats.22–26 The stability of THPs has allowed for their oral administration.27

The first generation THPIs were limited for potential in vivo applications, due to (a) thermal instability or (b) lack of selectivity. The melting temperature (T_m) of C_6-α1(V)GlyΨ-{PO_2H-CH_2}Val THPI was 25 °C, below that desired for a stable triple-helix under physiological conditions.12 The α1(I−III)GlyΨ{PO_2H-CH_2}Leu THPI was selective toward collagenolytic MMPs, but that group included seven enzymes. The present experiments were designed to overcome these structural and functional shortcomings by using “second” generation THPIs. First, we wished to increase the thermostability of the MMP-2/MMP-9 selective THPI for in vivo use. We utilized the non-native amino acids (2*S*,4*R*)-4-fluoroproline (Flp) and (2*S*,4*R*)-4-methylproline (mep) to create a more thermally stable α1(V)GlyΨ{PO_2H-CH_2}Val THPI. Moreover, we streamlined the synthetic routes for the synthesis of 9-fluorenylmethoxycarbonyl (Fmoc)-protected Flp (Figure 1, **4**) and mep (Figure 1, **5**), resulting in a more practical THPI synthesis. Second, we wished to develop THPIs that offered selectivity among the MMP collagenolytic enzymes. We applied two different approaches to obtain selective THPIs for MT1-MMP, utilizing data obtained from phage display generation of MT1-MMP selective substrates and combinatorial chemistry generation of MT1-MMP selective inhibitors. The resulting THPIs were tested in in vivo models of multiple sclerosis (MS) and sepsis.

Results

Improved Thermal Stability of α1(V)GlyΨ{PO_2H-CH_2}Val THPI

Our prior study established that a THPI, modeled on the type V collagen sequence Gly-Pro-Pro-Gly_{439}-Val_{440}-Val-Val-Gly-Glu-Gln, efficiently inhibited MMP-2 and MMP-9.12 However, that THPI had a T_m value of 25 °C, which was too low for in vivo applications. To produce a more stable analog, our strategy involved incorporating non-native amino acids that favor the preorganization of triple-helical structure.28 Flp offers greater stability than Hyp in the Yaa position of the triple-helix, while mep offers greater stability than Pro in the Xaa position.28,29 Fmoc-Flp (Figure 1, **4**) and Fmoc-mep (Figure 1, **5**) were synthesized in large scale. The Fmoc-GlyΨ{PO_2H-CH_2}Val phosphinate dipeptide building block [(*R,S*)-2-isopropyl-3-((1-(*N*-(Fmoc)amino)methyl)adamantyl-oxyphosphinyl)propanoic acid], Fmoc-Flp, and Fmoc-mep were then incorporated by solid phase methodology to assemble (Gly-Pro-Hyp)$_4$-Gly-mep-Flp-Gly-Pro-Pro-GlyΨ-{PO_2H-CH_2}Val-Val-Gly-Glu-Gln-Gly-Glu-Gln-Gly-Pro-Pro-Gly-mep-Flp-(Gly-Pro-Hyp)$_4$-NH_2 [designated α1(V)GlyΨ-{PO_2H-CH_2}Val [$mep_{14,32}$,$Flp_{15,33}$] THPI]. Both the Flp and the mep residues were positioned to minimize potential interactions with MMP active sites (see Discussion).

The circular dichroism (CD) spectrum of α1(V)GlyΨ-{PO_2H-CH_2}Val [$mep_{14,32}$,$Flp_{15,33}$] THPI was indicative of a collagen-like triple-helix with strong negative molar ellipticity

([Θ]) at λ = 212 nm and a positive [Θ] at λ = 225 nm (Figure 2). To examine the THPI thermal stability, [Θ] at λ = 225 nm was monitored as a function of increasing temperature. α1(V)GlyΨ{PO_2H-CH_2}Val [$mep_{14,32}$,$Flp_{15,33}$] THPI exhibited a cooperative transition indicative of the melting of a triple-helix to single strands (Figure 2). The T_m was determined to be 43.2 °C (Figure 2), which represents appropriate stability for in vivo studies.

α1(V)GlyΨ{PO_2H-CH_2}Val [$mep_{14,32}$,$Flp_{15,33}$] THPI was examined for inhibition of MMP-2 and MMP-9 hydrolysis of the Knight substrate [Mca-Lys-Pro-Leu-Gly-Leu-Lys-(Dnp)-Ala-Arg-NH_2].30 The THPI exhibited K_i values of 189 and 91 nM for MMP-2 and MMP-9, respectively, at 25 °C (Table 1). It is noteworthy that the inhibitory potency was less compared to the first generation THPI (Table 1). At 25 °C, α1(V)-GlyΨ{PO_2H-CH_2}Val [$mep_{14,32}$,$Flp_{15,33}$] THPI is ~87% folded (Figure 2, middle panel), while the first generation THPI is ~50% folded at this temperature.12 The decrease in inhibitory effect may be due to an enhancement in stability of the triple-helical structure, which could slow its destabilization/unwinding by MMP-2 and MMP-9. Alternatively, the decrease in activity could be due to the mep and/or Flp residues interacting unfavorably with the respective enzyme. At 37 °C, the K_i values for MMP-2 and MMP-9 were improved to 2 and 1 nM, respectively (Table 1). At this temperature the triple-helix is more “unwound” than at 25 °C (~64% folded), and the destabilized structure more favorably interacts with MMP-2 and MMP-9 (see Discussion). For MMP-9, the activity is comparable to the first generation THPI at 37 °C (Table 1). For MMP-2, the activity is better compared with the first generation THPI at 37 °C (Table 1). At 37 °C, the first generation THPI is ~17% folded.12 Thus, inhibitor interaction with MMP-2 and MMP-9 appears to require a balance of folded and unfolded states, although MMP-9 interaction with the triple-helix is less critical for activity than MMP-2.

MS Model

In the active stage of MS, CD4+ T-cells activated in the periphery penetrate the blood−brain barrier (BBB), recruit immune cells, initiate destruction of the myelin sheath, and cause axonal loss. Experimental autoimmune encephalomyelitis (EAE) is a well-established murine model of MS. During MS and in the EAE animal model, MMP-2 and MMP-9 are required at key stages of disease progression. They are assumed to act as effector molecules in the (a) generation of neuroantigens, (b) disruption of the BBB, and (c) invasion of inflammatory cells into the brain parenchyma.31–33

There are various versions of the EAE model that differ based on the applied neuroantigen and/or mouse strain. The most widely used EAE model is the chronic progressive model, in which C57BL/6J mice are immunized with myelin oligodendrocyte glycoprotein (MOG). In this model, days 7−10 approximate the time of T-cell activation and migration across the BBB which manifests as disease onset. Approximately 3−5 days after initial onset, maximum clinical severity is observed prior to a slight reduction and stabilization. In addition to the clinical severity, the concurrent weight loss represents a key indicator of disease progression. Weight loss is typically observed right before disease onset.34,35

EAE was induced herein with the MOG_{35-55} peptide. EAE mice were treated daily from day 7 with an intraperitoneal dosage of 12.43 μg of α1(V)GlyΨ{PO_2H-CH_2}Val [$mep_{14,32}$,$Flp_{15,33}$] THPI/animal. With a molecular weight of 12.4 kDa, one 12.43 μg dosage of α1(V)GlyΨ{PO_2H-CH_2}Val [$mep_{14,32}$,$Flp_{15,33}$] THPI corresponded to 1 μmol. Mice have ~58.5 mL of blood per kg of body weight. Hence, a mouse weighing 25 g would have a total blood volume (TBV) of ~58.5 mL/kg × 0.025 kg = 1.46 mL. Consequently, the blood concentration of α 1(V)Gly Ψ {PO_2H-CH_2}Val [$mep_{14,32}$,$Flp_{15,33}$] THPI would reach (1×10^{-6} mol)/(1.46×10^{-3} L) = 690 nM. This concentration is considerably higher than the α1(V)GlyΨ{PO_2H-CH_2}Val [$mep_{14,32}$,$Flp_{15,33}$] THPI K_i for MMP-9 (Table 1).

THPI treatment reduced the clinical severity of EAE from day 12 on (Figure 3A, Figure 3C). The THPI treated mice on average had less weight loss per day and increased their weight before the control group (Figure 3B, Figure 3D).

MT1-MMP Selectivity of THPIs

Of the two prior homotrimeric THPIs, C_6-α1(V)GlyΨ{PO_2H-CH_2}Val THPI did not inhibit MT1-MMP,12 while α1(I−III)GlyΨ{PO_2H-CH_2}Leu THPI inhibited MT1-MMP with K_i = 120 nM.15 Unfortunately, α1(I−III)GlyΨ{PO_2H-CH_2}Leu THPI is not selective for MT1-MMP, as it also effectively inhibits MMP-1, MMP-2, and MMP-9.14,15

Two screening approaches were used to obtain THPI sequences with greater selectivity for MT1-MMP. The first was based on a phage display data utilized to identify MT1-MMP substrates,36 and the second was based on a hydroxamic acid peptide combinatorial library utilized to obtain selective MMP inhibitors.37 Motifs from each of these studies were incorporated into THPs, starting from the general collagenolytic MMP substrate template $(Gly\text{-}Pro\text{-}Hyp)_5$-Gly-Pro-Gln-Gly~Leu-Arg-Gly-Gln-Arg-Gly-Val-Arg-$(Gly\text{-}Pro\text{-}Hyp)_5$-$NH_2$. The THP sequences, designations, and sources were as follows:

$(Gly\text{-}Pro\text{-}Hyp)_5$-Gly-**Arg**-**Ile**-Gly-**His**~**Leu**-**Arg**-**Thr**-Gln-Gly-Val-Arg-$(Gly\text{-}Pro\text{-}Hyp)_5$-Tyr-$NH_2$ (designated HLRT, phage display motif bolded);

$(Gly\text{-}Pro\text{-}Hyp)_5$-Gly-**Arg**-**Ile**-Gly-**Phe**~**Leu**-**Arg**-**Thr**-Gln-Gly-Val-Arg-$(Gly\text{-}Pro\text{-}Hyp)_5$-Tyr-$NH_2$ (designated FLRT, phage display motif bolded);

$(Gly\text{-}Pro\text{-}Hyp)_6$-Gly-Pro-Gln-Gly~**Val**-**Gln**-**His**-Gln-Arg-Gly-Val-Arg-$(Gly\text{-}Pro\text{-}Hyp)_5$-$NH_2$ (designated VQH, inhibitor motif bolded);

$(Gly\text{-}Pro\text{-}Hyp)_6$-Gly-Pro-Gln-Gly~**Val**-**Ser**-**Trp**-Gln-Arg-Gly-Val-Arg-$(Gly\text{-}Pro\text{-}Hyp)_5$-$NH_2$ (designated VSW, inhibitor motif bolded);

$(Gly\text{-}Pro\text{-}Hyp)_6$-Gly-Pro-Gln-Gly~**Ile**-**His**-**Lys**-Gln-Arg-Gly-Val-Arg-$(Gly\text{-}Pro\text{-}Hyp)_5$-$NH_2$ (designated IHK; inhibitor motif bolded)

$(Gly\text{-}Pro\text{-}Hyp)_6$-Gly-Pro-Gln-Gly~**Ile**-**Tyr**-**Phe**-Gln-Arg-Gly-Val-Arg-$(Gly\text{-}Pro\text{-}Hyp)_5$-$NH_2$ (designated IYF, inhibitor motif bolded);

$(Gly\text{-}Pro\text{-}Hyp)_5$-Gly-**Arg**-**Ile**-Gly-**Phe**~**Leu**-**Asp**-**Pro**-Gln-Gly-Val-Arg-$(Gly\text{-}Pro\text{-}Hyp)_5$-Tyr-$NH_2$ (designated FLDP, combined phage display and inhibitor motif bolded).

All THPs exhibited triple-helical CD spectra and cooperative melting curves (Figure S1 in Supporting Information). The THP melting temperatures were 27, 32, 42, 43, 39, 41, and 28 °C for HLRT, FLRT, VQH, VSW, IHK, IYF, and FLDP, respectively (Figure S1). The % folded at 25 °C was 72, 79, 87, 92, 83, 88, and 72 for HLRT, FLRT, VQH, VSW, IHK, IYF, and FLDP, respectively. Thus, all THPs were examined for their inhibitory potential of MT1-MMP at 25 °C, where the majority of the THP existed as a folded triple-helix. Only IHK and IYF showed good inhibitory activity at both concentrations tested (50 and 300 μM) (Figure 4).

The sequences of IHK and IYF were used to design two homotrimeric THPIs containing a Gly-Ile phosphinic dipeptide. The THPI sequences were (Gly-Pro-Hyp)$_4$-Gly-mep-Flp-Gly-Pro-Gln-{GlyΨ(PO_2H-CH_2)Ile}-Tyr-Phe-Gln-Arg-Gly-Val-Arg-Gly-mep-Flp-(Gly-Pro-Hyp)$_4$-Tyr-NH_2 (designated GlyΨ-{PO_2H-CH_2}Ile-Tyr-Phe-Gln THPI) and (Gly-Pro-Hyp)$_4$-Gly-mep-Flp-Gly-Pro-Gln-{GlyΨ(PO_2H-CH_2)Ile}-His-Lys-Gln-Arg-Gly-Val-Arg-Gly-mep-Flp-(Gly-Pro-Hyp)$_4$-Tyr-NH_2 (designated GlyΨ{PO_2H-CH_2}Ile-His-Lys-Gln THPI). Both THPIs exhibited triple-helical CD spectra and cooperative melting curves (Figure S2). GlyΨ{PO_2H-CH_2}Ile-Tyr-Phe-Gln THPI and GlyΨ{PO_2H-CH_2}Ile-His-Lys-Gln THPI had T_m values of 25.4 and 25.9 °C, respectively. These lower T_m values are not surprising when one considers the interruption of the Gly-Xaa-Yaa repeat in the sequences.

GlyΨ{PO_2H-CH_2}Ile-Tyr-Phe-Gln THPI and GlyΨ{PO_2H-CH_2}Ile-His-Lys-Gln THPI were initially tested for the inhibitory activity against MT1-MMP and MMP-8, as these two enzymes have similar THP sequence specificity profiles17,38 which complicates the development of selective MT1-MMP inhibitors. GlyΨ{PO_2H-CH_2}Ile-His-Lys-Gln THPI was a poor MT1-MMP inhibitor (Table 2). Surprisingly, GlyΨ{PO_2H-CH_2}Ile-His-Lys-Gln THPI effectively inhibited MMP-8 and MMP-1 with K_i values of 120 and 170 nM, respectively (Table 2), despite the design principles that, based on prior studies, would have predicted the opposite outcome.37 GlyΨ{PO_2H-CH_2}Ile-Tyr-Phe-Gln THPI was an excellent MT1-MMP inhibitor (Table 2). However, GlyΨ{PO_2H-CH_2}Ile-Tyr-Phe-Gln THPI inhibited all collagenolytic MMPs tested (Table 2) In fact, GlyΨ{PO_2H-CH_2}Ile-Tyr-Phe-Gln THPI was an outstanding MMP-9 inhibitor and demonstrated almost 1000-fold better inhibition of MMP-9 compared with MMP-2 (Table 2). While the thermal stabilities of GlyΨ{PO_2H-CH_2}Ile-Tyr-Phe-Gln THPI and GlyΨ{PO_2H-CH_2}Ile-His-Lys-Gln THPI were lower than desired for in vivo experiments, the low levels of MMP-3 inhibition (Table 2) indicated selectivity against noncollagenolytic proteases.

Sepsis Model

MMP-8 gene expression and activity are increased in human sepsis, and the degree of increase is associated with worsening clinical outcome.39,40 Genetic ablation or pharmacological inhibition of MMP-8 conferred a survival advantage in an animal model of sepsis.40 In turn, ablation of MT1-MMP in an animal model of endotoxemia and decreased MT1-MMP in human sepsis resulted in an increased proinflammatory response, more severe lung injury, and increased mortality.41 GlyΨ{PO_2H-CH_2}Ile-His-Lys-Gln THPI was an effective MMP-8 inhibitor and offered 40-fold selectivity between MMP-8 and MT1-MMP (Table 2). GlyΨ{PO_2H-CH_2}Ile-His-Lys-Gln THPI was thus applied to a murine model of

sepsis. We used the cecal ligation and puncture (CLP) sepsis model, which entails opening the abdomen, ligating the cecum, and puncturing the cecum with a needle to induce bacterial peritonitis. The severity can be controlled depending on the size of the needle and the number of punctures.

A dosage of 10 mg of GlyΨ{PO_2H-CH_2}Ile-His-Lys-Gln THPI per kg was chosen for the sepsis model. With a molecular weight of 12.6 kDa, a delivery of 10 mg of GlyΨ{PO_2H-CH_2}Ile-His-Lys-Gln THPI per kg corresponded to 0.79 mmol/kg, assuming an average mouse weight of 25 g results in delivery of 19.75 μmol per mouse. By use of the earlier calculation of TBV of ~1.46 mL, the concentration of GlyΨ{PO_2H-CH_2}Ile-His-Lys-Gln THPI would be $(19.75 \times 10^{-6}$ mol)/$(1.46 \times 10^{-3}$ L) = 13.5 μM. This concentration is considerably higher than the GlyΨ{PO_2H-CH_2}Ile-His-Lys-Gln THPI K_i for MMP-8 (Table 2).

Following CLP, none of the nontreated wild-type mice survived after 7 days, while 70% of the wild-type mice treated with GlyΨ{PO_2H-CH_2}Ile-His-Lys-Gln THPI survived after 7 days (Figure 5). Thus, treatment of wild-type mice with GlyΨ{PO_2H-CH_2}Ile-His-Lys-Gln THPI after CLP conferred a significant survival advantage. To examine the specificity of the THPI in vivo, Mmp8 null mice underwent CLP and were then either treated with the THPI or not treated. A survival advantage during sepsis was observed for Mmp8 null mice compared with wild-type mice (Figure 5 gray line versus Figure 6 gray line). Survival of inhibitor treated wild-type mice mirrored that of nontreated Mmp8 null mice (Figure 5 black line versus Figure 6 gray line), while survival of Mmp8 null mice was not augmented by inhibitor treatment (Figure 6 gray versus black line). Thus, the THPI appears to be acting specifically toward MMP-8 in vivo.

We next examined potential modes of action of the THPI. Bacterial colony counts in blood 24 h after CLP were not different between the wild-type treated and nontreated groups (Figure S4), suggesting that the THPI was not acting through an antibacterial mechanism. The lung is an important distal organ of injury in clinical sepsis and is recapitulated in the CLP model.40 Neutrophil invasion into the lungs was quantified by determining lung myeloperoxidase (MPO) activity. The improvement in survival was found to be correlated with significantly decreased MPO activity (Figure 7) and hence neutrophil infiltration into the lungs. The inflammatory cytokine profiles in these mice were next studied. There was no effect on interleukin 1β (IL-1β), IL-6, keratinocyte chemoattractant (KC, also known as CXCL1), or LPS-induced CXC chemokine (LIX) levels upon GlyΨ{PO_2H-CH_2}Ile-His-Lys-Gln THPI treatment (Figure S3). Increased levels were observed for TNF-α, macrophage inflammatory protein 1 (MIP-1, also known as CCl3 + CCL4), and IL-10 following GlyΨ{PO_2H-CH_2}Ile-His-Lys-Gln THPI treatment (Figure 8).

Discussion

THPI Treatment of MS

The design of MMP inhibitors has been significantly improved by the integration of secondary binding sites (exosites). Exosite binding peptides and small molecules have been described as selective MT1-MMP inhibitors.42 Selective antibodies have also been

developed for MMP-9 and MT1-MMP based on binding to exosites.43–49 Finally, allosteric, small molecule inhibitors of MMP-13 are well documented.50–61

The development of collagen helical model THPIs is based on the concept that collagenolytic MMPs will have distinct exosites from noncollagenolytic MMPs and, thus, that this class of inhibitors will exhibit selectivity within the MMP family. Further fine-tuning of the sequence, based on studies with triple-helical peptide substrates,17,38,62–64 would enhance selectivity. However, two key problems were associated with the first generation of THPIs. First, the incorporation of the phosphinate significantly decreased the triple-helical stability of the constructs compared with the analogous substrates.12,14 Second, triple-helical peptide studies did not always provide selective sequences.

Our initial MMP-2/MMP-9 THPI offered excellent selectivity toward those two MMPs but inadequate thermal stability.12 To overcome this weakness, the present studies incorporated non-native amino acids in an attempt to enhance inhibitor stability. Flp and mep, in the Yaa and Xaa positions of the triple-helix, respectively, favor the preorganization of triple-helical structure.28 Because the phosphinate moiety destabilizes the triple-helix, the Flp and mep residues needed to be incorporated near the phosphinate but not in subsites that might result in detrimental interactions with the enzymes (MMP-2 and MMP-9). Flp was incorporated at the P_5 and $P_{14}{}'$ subsites, while mep was incorporated at the P_6 and $P_{13}{}'$ subsites. The first generation THPI had Hyp and Pro at these subsites, respectively.12 Due to the structural similarity of Flp to Hyp and mep to Pro, these substitutions were not anticipated to produce significant unfavorable interactions with MMP-2 and MMP-9. Ultimately, the judicious use of two Flp and two mep residues (per strand) greatly improved THPI thermal stability (ΔT_m = 18 °C). The resulting inhibitor (α1(V)GlyΨ-{PO_2H-CH_2}Val [$mep_{14,32}$,$Flp_{15,33}$] THPI) was less effective than the parent inhibitor at 25 °C, most likely due to less mobility of the individual peptide strands. Models of MMP-2/MMP-9 collagenolysis suggest that the triple-helix needs to be substantially unwound locally to facilitate hydrolysis of the strands.65 However, the activity of the inhibitor was excellent at 37 °C, the appropriate temperature for in vivo studies.

Treatment with the α1(V)GlyΨ{P O_2 H-CH_2 }Val [$mep_{14,32}$,$Flp_{15,33}$] THPI in the EAE mouse model resulted in reduction of clinical severity and weight loss per day, both of which are hallmarks of EAE. There are numerous indications for the role of MMP-9, and perhaps MMP-2, in MS.66,67 MMP-9 levels are elevated in MS serum and cerebrospinal fluid, particularly in patients with active disease.32,68–70 Injection of MMP-9 into the brain causes disruption of the basement membrane and is associated with breakdown of the BBB.71,72 In MS patients, leukocyte-derived MMP-9 facilitates leukocyte penetration of the BBB.67 Concurrent knockout of MMP-2 and MMP-9 results in the inability to induce EAE in mice,73 while loss of MMP-9 alone leaves young (but not older) mice significantly less susceptible to EAE.31,74 Hydrolysis of dystroglycan by MMP-2 and MMP-9 promotes leukocyte penetration of the parenchymal basement membrane during EAE.73 Inhibitory activities for C_6-α1(V)GlyΨ{PO_2H-CH_2}Val THPI were similar for full-length (82 kDa) MMP-9 or TIMP-1 resistant (65 kDa) MMP-914 and coincide with the finding that TIMP-1 resistant MMP-9 appears to be the predominant enzyme form contributing to MS.75

THPI Treatment of Sepsis

Our initial THPI that was designed based on interstitial collagen hydrolysis offered no selectivity among the collagenolytic MMPs.14,15,76 Creating heterotrimeric analogs resulted in THPIs that did not inhibit MMP-1 but were still not selective within the remaining collagenolytic MMPs.15 Expression of MT1-MMP has been associated with a variety of cellular and developmental processes, as well as multiple physiopathological conditions. MT1-MMP is also known to convert pro-MMP-2 to active protease and to cleave a number of matrix proteins including collagen, fibronectin, and vitronectin. In an attempt to obtain an MT1-MMP selective THPI, we utilized prior studies that described MT1-MMP selective single-stranded peptides and inhibitors. Unfortunately, those selectivities did not translate to triple-helical constructs. A similar observation was made previously.38 Fortuitously, GlyΨ{PO_2H-CH_2}Ile-His-Lys-Gln THPI, which was not particularly effective toward MT1-MMP but was a good MMP-8 inhibitor, could be applied in an in vivo sepsis model.

High serum or plasma levels of MMP-8 correlate to sepsis severity and fatality.39,40 Protection from endotoxin shock following LPS challenge was observed in mice treated with peptidic inhibitors of MMP-8 and MMP-9, and an MMP-8 selective nanobody.77–79 MMP-8 has been indicated to be a key mediator in the regulation of innate immunity.80 The three inflammatory cytokines constituting the “cytokine storm” during septic shock are IL-1β, IL-6, and TNF-α, and recent studies have implicated IL-3.81 Comparison of CLP in wild type and Mmp8 knockout mice showed no difference in increases of KC, MIP-1α and TNF-α, while LIX did not increase in either model.40 The increase in wild-type mice IL-6 was reduced and the increase in wild-type mice IL-1β was completely eliminated in the knockout mice.40 Thus, the septic shock increase of IL-6 and IL-1β observed in the wild-type mouse CLP model was positively correlated to MMP-8 concentration.

In contrast to the observations in the Mmp8 knockout mice 6 h after CLP,40 the cytokine storm was only partially affected by GlyΨ{PO_2H-CH_2}Ile-His-Lys-Gln THPI treatment. Differences observed between THPI treatment and Mmp8 knockout may have several origins. First, Mmp8 deletion removed all MMP-8 activity, while the THPI presumably reduced, but did not eliminate, MMP-8 activity. Second, global Mmp8 deletion may induce a background environment in the mouse that had not been previously appreciated. Third, the THPI may interact with alternative targets, resulting in pleiotropic effects. Dose–response testing of the THPI may yield insights into the origin(s) of the differences.

Prior treatment of CLP mice with a small molecule inhibitor designed for MMP-8 ((3*R*)-(+) - [2 -(4-methoxy-benzenesulfonyl)-1,2,3,4-tetrahydroisoquinoline-3-hydroxamate], whose true selectivity was not studied),82 reduced whole lung MPO activity and improved survival, 40 consistent with observations here. However, this inhibitor significantly reduced IL-6, IL-1β, MIP-1α, and TNF-α while increasing IL-10.40 GlyΨ{PO_2H-CH_2}Ile-His-Lys-Gln THPI is potentially more selective than the previously used hydroxamate, which may explain the observed differences in cytokine regulation.

IL-10 is an anti-inflammatory cytokine.83 It was significantly elevated in the THPI treated CLP mice, compared to the vehicle treated CLP mice. This suggested that treatment with the

THPI altered the balance of pro-/anti-inflammatory cytokines toward a “less inflamed” response to sepsis and is consistent with the paradigm of overwhelming inflammation being deleterious in sepsis. Whether this is a direct effect of MMP-8 inhibition or some nonspecific effect of the THPI is unknown.

Several additional roles for MMP-8 in sepsis have been suggested. MMP-8 efficiently cleaves IL-13, inactivating it.84 MMP-8 cleaves the N-terminus of LIX, CXCL8, and CXCL5, increasing their activity including enhancement of polymorphonuclear neutrophil chemotaxis.80 However, we observed no effect on LIX using GlyΨ{PO_2H-CH_2}Ile-His-Lys-Gln THPI. MMP-8 directly activates NF-kB, which may lead to regulation of the inflammatory state.40 MMP-8 may also be acting indirectly by cleaving and inactivating α1-protease inhibitor, which in turn increases the presence of active neutrophil elastase.85 Neutrophil elastase can directly damage lung tissue.86

Conclusions

THPIs hold great promise as probes of enzyme activity and imaging agents. THPs have excellent stability in vivo.22,24,27 Phosphinic peptides designed as MMP inhibitors also exhibit favorable in vivo properties.87 The α1(V)GlyΨ{PO_2H-CH_2}Val [$mep_{14,32}$,$Flp_{15,33}$] THPI described herein is sufficiently stable to adopt primarily a triple-helical structure in vivo. The triple-helical structure facilitates binding of the inhibitor to the targeted MMPs while minimizing proteolytic degradation. Although MMP-9 selective, inhibitory antibodies and antibody fragments have been described,47,48,88–91 their application for neurological disorders is limited based on the inability of antibodies to cross the BBB. The effectiveness of the MMP-2/MMP-9 α1(V)GlyΨ{PO_2H-CH_2}Val [$mep_{14,32}$,$Flp_{15,33}$] THPI in the EAE mouse model indicated that this inhibitor *may* cross the BBB. Subsequent studies will address the efficiency of THPI delivery across the BBB and the integrity of the BBB during EAE.

While our attempt to design a selective MT1-MMP THPI was not successful, we did obtain a THPI that was effective in the CLP animal model of sepsis, most likely through targeting of MMP-8. Although the GlyΨ{PO_2H-CH_2}Ile-His-Lys-Gln THPI had low triple-helical thermal stability, it retained selectivity as indicated by its lack of inhibition of MMP-3 and most likely did not undergo general proteolysis in vivo. Gly-Pro-Hyp repeats themselves are stable in human serum26 and thus prevent exopeptidase and possibly inhibit endopeptidase action toward the THPI. The intestine has been found to be the source of MMP-8 in septic peritonitis.92 The application of MMP-8 inhibitors such as GlyΨ{PO_2H-CH_2}Ile-His-Lys-Gln THPI could be considered in abdominal sepsis associated with intestinal injury92 and in adult, rather than juvenile, patients.93

Experimental Section

Chemistry, General

All reactions were carried out under an inert atmosphere and anhydrous conditions with dry solvents unless otherwise stated. Analytical thin layer chromatography was performed on 0.25 mm silica gel 60-F plates. Visualization was accomplished with UV light and aqueous

potassium permanganate solution staining followed by air drying. Purification of reaction products was carried out using flash silica gel 40–63 μm. All the standard chemicals and reagents are commercially available and were used without further purification.

All standard peptide synthesis chemicals were peptide synthesis grade. *N*,*N*-Dimethylformamide (DMF), trifluoroacetic acid (TFA), dichloromethane (DCM), and ethyl acetate (EtOAc) were purchased from Fisher Scientific (Pittsburgh, PA). *N*-Methylmorpholine (NMM), 1,8-diazabicyclo[5.4.0]undec-7-ene (DBU), and triisopropylsilane were purchased from Acros Organics. 2-(6-Chloro-1*H*-benzotriazole-1-yl)-1,1,3,3-tetramethylaminium hexafluorophosphate (HCTU) was purchased from Anaspec. All Fmoc-amino acid derivatives and Nova PEG Rink amide resin were purchased from Novabiochem. Amino acids are of L-configuration (except for Gly).

^{1}H NMR spectra were recorded on a Varian Mercury 400 (400 MHz) spectrometer and are reported in ppm using solvent as an internal standard ($CDCl_3$ at 7.26 ppm). Data are reported as (b = broad, s = singlet, d = doublet, t = triplet, q = quartet, p = pentet, m = multiplet; coupling constant(s) in Hz, integration). ^{13}C NMR were recorded on Varian Mercury 400 (100 MHz) spectrometer. Chemical shifts are reported in ppm, with solvent resonance employed as the internal standard ($CDCl_3$ at 77.0 ppm). High-resolution mass spectra were obtained from the University of Florida Mass Spectrometry Laboratory.

THPIs were obtained in ≥95% purity as determined by RP-HPLC on a Vydac C_{18} column (5 μm, 300 Å, 150 mm × 4.6 mm) at a flow rate of 1 mL/min. The elution gradient was 2–98% of B in 20 min (where A is 0.1% TFA in water and B is 0.1% TFA in CH_3CN), and detection was at λ = 220 nm.

The synthesis of Fmoc-Gly-Val phosphinate dipeptide [(*R*,*S*)-2-isopropyl-3-((1-(*N*-(Fmoc)amino)methyl)adamantyloxyphosphinyl)-propanoic acid] (Figure 1, **3a**) started from commercially available materials and followed an efficient bis-deprotection strategy as the key step.94 Fmoc-Gly-Ile phosphinic dipeptide [(*R*,*S*)-2-(2-butyl)-3-((1-(*N*-(Fmoc)amino)methyl)adamantyloxyphosphinyl)propanoic acid] (Figure 1, **3c**) was prepared as previously described.95

To efficiently incorporate Flp and mep into a peptide sequence, convenient synthetic routes for the preparation of Fmoc-Flp (Figure 1, **4**) and Fmoc-mep (Figure 1, **5**) were required. We recently reported a convenient synthetic route for the preparation of Fmoc-Flp from readily available, inexpensive *trans*-(4*R*)-hydroxy-L-proline.96 The fluorination step was modified herein. Morpholinosulfur trifluoride (3.8 mL, 31.2 mmol) was added dropwise to a solution of *N*-benzyloxycarbonyl (Cbz)-*trans*-(4*S*)-hydroxy-L-proline-*O*-benzyl (Bzl) (3.7 g, 10.4 mmol) in dry DCM (50 mL) at −78 °C under argon atmosphere. The reaction mixture was stirred for additional 1 h at −78 °C and allowed to warm to room temperature. After 24 h, the reaction mixture was carefully quenched with saturated aqueous $NaHCO_3$ solution. The organic layer was separated and washed with water (2 × 75 mL) and dried over anhydrous Na_2SO_4. Solvent evaporation under reduced pressure followed by flash chromatography using hexanes/EtOAc (4:1) yielded pure *N*-Cbz-(4*R*)-Flp-OBzl as light yellow gummy liquid (1.87 g, 50%). ^{1}H NMR (500 MHz, $CDCl_3$): δ 2.0–2.25 (m, 1H), 2.40–2.70 (m, 1H),

3.55–3.80 (m, 1H), 3.85–4.15 (m, 1H), 4.45–4.70 (m, 1H), 4.95–5.40 (m, 4H), 7.20–7.40 (m, 10H). A one-pot three-step procedure involving a bis-deprotection of the N- and C-termini of *N*-Cbz-4(*R*)-Flp-OBzl under catalytic hydrogenation conditions followed by selective protection of the N-terminus with an Fmoc group was employed to yield Fmoc-Flp.96

To obtain Fmoc-mep, *N*-Boc-*trans*-mep was initially synthesized as reported by Del Valle and Goodman.97 Fmoc group installation was achieved according to the procedure described by Shoulders et al.98

Peptide Synthesis and Purification

The solid-phase synthesis of THPs was performed using Fmoc chemistry on either a Protein Technologies PS3 or CEM Liberty automated microwave peptide synthesizer as described99 with Nova PEG Rink amide resin (loading of 0.44 mmol/g except for FLDP, where loading was 0.5 mmol/g). For assembly of FLRT and IHK on the Liberty, coupling was achieved with 5.0 equiv of each amino acid, 4.9 equiv of HCTU (0.5 M in DMF), and 8.0 equiv of NMM (2 M in DMF) at 25 W, 50 °C for 300 s (double coupling for all Arg residues first at 0 W, 25 °C for 25 min followed by 25 W, 50 °C for 300 s and FLRT Pro11 and IHK Pro32 at 25 W, 50 °C for 300 s twice), while deprotection was achieved by treatment with 20% piperidine in 0.1 M HOBt/DMF initially at 35 W, 75 °C for 30 s followed by 35 W, 75 °C for 180 s. For assembly of HLRT and FLDP on the Liberty, coupling was achieved with 5.0 equiv of each amino acid, 4.9 equiv of HCTU (0.5 M in DMF), and 8.0 equiv of NMM (2 M in DMF) at 25 W, 50 °C for 300 s (double coupling for all Arg residues first at 0 W, 25 °C for 25 min followed by 25 W, 50 °C for 300 s and Pro11 at 25 W, 50 °C for 300 s twice), while deprotection was achieved by treatment with 10% piperazine in DMF initially at 35 W, 75 °C for 30 s followed by 35 W, 75 °C for 180 s. For assembly of VQH, VSW, and IYF on the PS3, coupling was achieved with 4.0 equiv of each amino acid, 3.9 equiv of HCTU, and 8.0 equiv of NMM (0.4 M in DMF) for 30 min (double coupling for VQH Pro8, VSW and IYF Pro14), while deprotection was achieved by treatment with 1% DBU, 5% piperidine in DMF 3 times for 6 min each.

Side chain deprotection and cleavage of all THPs from the resin were achieved by two treatments with H_2O–thioanisole–EDT–TFA (5:5:2.5:87.5) for 3 h each in Ar. THPs were purified by RP-HPLC (see below) and characterized by matrix-assisted laser desorption/ionization time-of-flight mass spectrometry as described99 using an Applied Biosystems Voyager DE-PRO. $[M + H]^+$ values for THPs were 4183.4 Da for HLRT (theoretical 4184.64 Da), 4195.6 for FLRT (theoretical 4194.67 Da), 4261.1 Da for VQH (theoretical 4257.63 Da), 4267.0 Da for VSW (theoretical 4265.65 Da), 4272.8 Da for IHK (theoretical 4271.72), 4318.9 Da for IYF (theoretical 4316.75 Da), and 4150.8 Da for FLDP (theoretical 4149.59 Da).

The solid-phase synthesis of GlyΨ{PO_2H-CH_2}Ile-His-Lys-Gln THPI and GlyΨ{PO_2H-CH_2}Ile-Tyr-Phe-Gln THPI was performed on a CEM Liberty automated microwave peptide synthesizer using Nova PEG Rink amide resin (loading 0.5 mmol/g) utilizing Fmoc chemistry. The coupling of usual Fmoc-amino acids was achieved with 5 equiv of each amino acid, 4.9 equiv of HCTU (0.5 M in DMF), and 8.0 equiv NMM (2 M in DMF) using

microwave power of 25 W at 50 °C with the reaction time of 300 s (double coupling for all Arg residues first at 0 W, 25 °C for 25 min followed by 25 W, 50 °C for 300 s). The removal of Fmoc-protecting group was accomplished using 10% piperazine in DMF (microwave power of 35W at 75 °C and the reaction time of 30 s, followed by a second treatment under the same conditions for 180 s). The unusual amino acids, Fmoc-Flp-OH and Fmoc-mep-OH, were coupled using 3 equiv of amino acid, 2.9 equiv of HCTU, and 6 equiv of NMM with microwave power of 25 W at 50 °C for 300 s. The coupling of Fmoc-mep-OH was repeated. The Fmoc-protected phosphinic dipeptides were attached using 3 equiv of dipeptide, 3 equiv of DIPCDI, 6 equiv of HOBt, and DIPEA to adjust pH to ~8 at 40 °C for 40 min and room temperature overnight. Following dipeptide addition the peptide-resin was capped using 0.5 M Ac_2O, 0.125 M DIPEA, and 0.015 M HOBt in DMF at room temperature for 1 h. The deprotection of Fmoc group, immediately after incorporation of the phosphinic dipeptide into the sequence, was performed without microwave power but with increased reaction times of 500 and 800 s. The amino acid immediately after the dipeptide was attached using the same conditions as for the dipeptide; Pro11 was double coupled.

The solid-phase synthesis of α1(V)GlyΨ{PO_2H-CH_2}Val [$mep_{14,32}$,$Flp_{15,33}$] THPI was performed on a CEM Liberty Blue automated microwave peptide synthesizer using Nova PEG Rink amide resin (loading 0.48 mmol/g) utilizing Fmoc chemistry. The coupling of usual Fmoc-amino acids was achieved with 5 equiv of each amino acid (0.2 M), 5 equiv of DIPCDI (0.5 M in DMF), and 5 equiv of oxyma (1 M in DMF). Fmoc-amino acid coupling cycles were carried out for 15 s at 75 °C and 110 s at 90 °C. Fmoc deprotection was achieved with 10% piperazine (w/v) in ethanol/*N*-methyl-2-pyrrolidone (10:90) for 15 s at 75 °C and 50 s at 90 °C. Fmoc-Flp-OH was incorporated using 2.5 equiv of amino acid for 600 s at 25 °C and 300 s at 75 °C. Fmoc-mep-OH and Fmoc-GlyΨ{PO_2H-CH_2}Val were incorporated using 2.5 equiv of each compound for 1500 s at 25 °C and 600 s at 75 °C. Coupling of Fmoc-Pro-OH following GlyΨ{PO_2H-CH_2}Val was performed for 1500 s at 25 °C and 600 s at 75 °C for using 5 equiv of amino acid. For all THPIs, the final cleavage of peptide from the resin and side chain deprotection were carried out using 7 mL of triisopropylsilane–phenol–H_2O–TFA (2:5:5:88) under inert atmosphere (Ar) for 3 h.

THPs and phosphinic peptides were purified using RP-HPLC on a Vydac C_{18} column (15–20 μm, 300 Å, 250 mm × 22 mm) at a flow rate of 10 mL/min. The elution gradients were 7–30% of B in 40 min [for GlyΨ{PO_2H-CH_2}Ile-His-Lys-Gln THPI], 10–35% of B in 50 min [for GlyΨ{PO_2H-CH_2}Ile-Tyr-Phe-Gln THPI], and 20–50% of B in 30 min [for α1(V)GlyΨ{PO_2H-CH_2}Val [$mep_{14,32}$,$Flp_{15,33}$] THPI] (where A is 0.1% TFA in water and B is 0.1% TFA in CH_3CN) and detection was at λ = 220 nm. Homogenous fractions were combined and lyophilized. Purified THPIs were characterized by matrix-assisted laser desorption/ionization time-of-flight mass spectrometry as described12,15 using an Applied Biosystems Voyager DE-PRO or Bruker microflex workstation. $[M + H]^+$ values for THPIs were 4145.3 Da for α1(V)GlyΨ{PO_2H-CH_2}Val [$mep_{14,32}$,$Flp_{15,33}$] THPI (theoretical 4143.36 Da), 4235.5 Da for GlyΨ{PO_2H-CH_2}Ile-His-Lys-Gln THPI (theoretical 4234.64 Da), and 4280.5 Da for GlyΨ{PO_2H-CH_2}Ile-Tyr-Phe-Gln THPI (theoretical 4279.00 Da).

CD Spectroscopy

CD spectra were recorded over the range λ = 190–250 nm on a JASCO J-810 spectropolarimeter using a 10 mm path length quartz cell. The thermal transition curves were obtained by recording the molar ellipticity ([Θ]) at 225 nm, while the temperature was continuously increased in the range of 5–85 °C at a rate of 15 °C/h. The temperature was controlled using a JASCO PTC-348WI temperature control unit. For samples exhibiting sigmoidal melting curves, the inflection point in the transition region (first derivative) is defined as the T_m. Alternatively, T_m was evaluated from the midpoint of the transition.

MMPs

Human recombinant, full-length proMMP-1, proMMP-3, proMMP-8, proMMP-13, and proMT1-MMP were purchased from R&D Systems (Minneapolis, MN) and activated prior to use. Trypsin-3 and 4-(2-aminoethyl)benzensulfonyl fluoride hydrochloride (AEBSF) were also purchased from R&D Systems. *p*-Aminophenylmercuric acetate was purchased from EMD Biosciences (San Diego, CA), and trypsin (TPCK-treated) was purchased from Worthington Biochemical Corporation (Lakewood, NJ). Recombinant MMP-2 and MMP-9 catalytic domains were purchased from R&D Systems and used directly without further activation in the desired concentration.

ProMMP-1, proMMP-3, proMMP-8, and proMMP-13 were activated by mixing an equal volume of stock enzyme solution and activator (*p*-aminomercuric acetate to a final concentration of 1 mM) followed by a 2–3 h incubation in a 37 °C water bath. ProMMP-2 was activated by incubating with 2 mM *p*-aminomercuric acetate for 1 h at 37 °C. ProMT1-MMP was activated by using trypsin-3 at a final concentration of 0.1 μg/mL and incubating for 1 h at 37 °C. The reaction was stopped by addition of AEBSF (at a final concentration of 1 mM) and incubation for 15 min at room temperature. Activated MMPs were diluted to 20–100 nM in ice cold TSB*Zn (50 mM Tris, 100 mM NaCl, 10 mM $CaCl_2$, 0.05% Brij-35, 0.02% NaN_3, 1 μM $ZnCl_2$, pH 7.5) to prevent autoproteolysis. Enzyme aliquots were kept on wet ice and used the same day. MMP activity was initially evaluated by using the Knight substrate and compared with prior data.14,76 In this way, activity toward the substrate was used as an indicator of enzyme integrity, rather than TIMP titration, as performed previously.17

Inhibition Kinetic Studies

Peptide substrate and inhibitor solutions were prepared using TSB*Zn. For testing THPs as inhibitors, 1–2 nM enzyme was incubated with varying concentrations of THPs for 2 h at room temperature. A 2 h incubation was utilized based on our prior studies using peptidic inhibitors of MMPs.100 Residual enzyme activity was monitored by adding fTHP-15 solution in TSB*Zn to produce a final concentration of $<0.1K_M$. Initial velocity rates were determined from the first 20 min of hydrolysis when product release is linear with time. Fluorescence was measured on a Bio-Tek Synergy H1 reader or H4 hybrid reader using $\lambda_{excitation}$ = 324 nm and $\lambda_{emission}$ = 393 nm. Apparent K_i values were calculated using SigmaPlot by fitting data to the equation $v = v_0/(1 + I/K_i)$, where v_0 is the activity in the absence of inhibitor and K_i is the apparent inhibition constant. Because the substrate

concentration is less than $K_M/10$, apparent K_i values are insignificantly different from true K_i values.

For THPIs, 1−2.5 nM enzyme was incubated with varying concentration of inhibitor for 2 h at room temperature or 37 °C. A 2 h incubation was utilized based on the generally observed behavior of slow on and off rates for tight-binding inhibitors101 and studies demonstrating that high affinity phosphinate inhibitors of Zn^{2+} metalloproteinases are slow binding.102 Residual enzyme activity was monitored by adding Knight substrate solution in TSB*Zn to produce a final concentration of $<0.1K_M$. Initial velocity rates were determined from the first 10 min of hydrolysis when product release is linear with time. Fluorescence was measured on a Bio-Tek Synergy H1 reader or H4 hybrid reader using $\lambda_{excitation}$ = 324 nm and $\lambda_{emission}$ = 393 nm. Apparent K_i values were calculated from the following formulas:12

$$\frac{v_i}{v_0} = \frac{E_t - I_t - K_i^{(app)} + ((E_t - I_t - K_i^{(app)})^2 + 4E_tK_i^{(app)})^{0.5}}{2E_t} \quad (1)$$

$$K_i^{(app)} = K_i\left(\frac{A_t + K_M}{K_M}\right) \quad (2)$$

where I_t is the total inhibitor concentration, E_t is the total enzyme concentration, A_t is the total substrate concentration, v_0 is the activity in the absence of inhibitor, and K_M is the Michaelis constant. In our assays the value of $E_t/K_i^{(app)}$ does not exceed 100 so that the inhibitor is distributed in both free and bound forms, and $K_i^{(app)}$ can be calculated by fitting inhibition data to eq 1. Because the substrate concentration is less than $K_M/10$, $K_i^{(app)}$ values are insignificantly different from true K_i values. In cases where weak inhibition occurred, $K_i^{(app)}$ values were calculated using $v_i = v_0/(1 + I_t/K_i^{(app)})$.

Murine Model of MS

All procedures involving animals were performed in accordance to the guidelines of the Institutional Animal Care and Use Committee. Complete Freund's adjuvant (CFA) was produced by emulsifying incomplete Freund's adjuvant (Thermo Scientific) and *M. tuberculosis* H37Ra (Becton Dickinson, Franklin Lakes, NJ). $MOG_{35–55}$ peptide (Met-Glu-Val-Gly-Trp-Tyr-Arg-Ser-Pro-Phe-Ser-Arg-Val-Val-His-Leu-Tyr-Arg-Asn-Gly-Lys-OH) was synthesized using standard Fmoc solid-phase chemistry103 and RP-HPLC purified to >90%. EAE was induced in female C57BL/6J mice (Jackson Laboratory; 10–12 weeks of age) by subcutaneously inoculating an emulsification of CFA and the $MOG_{35–55}$ peptide (200 μg/mouse) on day 0. Pertussis toxin (Hooke's Laboratory, 320 ng) was introduced via intraperitoneal injection 3 and 24 h later. The control group received phosphate buffered saline (PBS)/animal/day, while the treated group received 12.43 μg of α1(V)Gly**Ψ**{PO_2H-CH_2}Val [$mep_{14,32}$,$Flp_{15,33}$] THPI/animal per day by intraperitoneal injection. Disease severity (scored based on the Hooke's Laboratory scoring guide (www.hookelabs.com/

protocols/eaeAI_C57BL6.html)) and weight change were recorded from day 5 until sacrifice.

Murine Model of Sepsis

All experimental procedures involving mice complied with the Guide for the Care and Use of Laboratory Animals published by the U.S. National Institutes of Health (NIH Publication No. 85-23, revised 1996) and met approval of the Cincinnati Children's Research Foundation Institutional Animal Care and Use Committee. Mmp8–/– mice on a C57BL/6J background were provided by Dr. Steven Shapiro, University of Pittsburgh. Loss of the Mmp8 gene was confirmed by PCR using Mmp8 specific primers (data not shown). Wild type C57BL/6J mice were obtained from Harlan Laboratories (Indianapolis, IN). All mice were fed standard rodent chow and maintained on 12 h light–dark cycles.

Male mice aged 5–9 weeks underwent CLP as previously described.40 Briefly, mice were anesthetized and a midline laparotomy was performed. The cecum was isolated and ligated to 30% original diameter using 3–0 silk suture (Ethicon, Cincinnati, OH). Two through and through cecal perforations were made distal to the ligation using a 21-gauge needle, and a small amount of fecal content was expressed from each site. The cecum was then returned to the abdominal cavity, and the peritoneum was closed using 7–0 silk suture (Ethicon), followed by skin closure with surgical glue (Abbott Laboratories, Abbott Park, IL). Mice treated with vehicle received an intraperitoneal injection of PBS at a dose of 10 mL/kg after abdominal closure. The GlyΨ{PO_2H-CH_2}Ile-His-Lys-Gln THPI was dissolved in PBS to a final inhibitor concentration of 10 mg/mL. Animals received a 10 mg/kg dose of inhibitor immediately following abdominal closure. All mice received 0.6 mL of normal saline subcutaneously in the nape of the neck at the conclusion of the operation. Animals were redosed with the THPI or PBS vehicle at 12 h intervals, for up to 5 additional doses. Following CLP, animals were monitored for survival up to 7 days or were sacrificed at 24 h to procure lung and blood samples.

Measurement of Myeloperoxidase Activity

MPO was measured as an indication of neutrophil infiltration in lung tissue, as previously described.104 Briefly, whole lung tissue was homogenized and myeloperoxidase activity was assessed using spectrophotometry and defined as the quantity of enzyme degrading 1 μmol of hydrogen peroxide/min at 37 °C, expressed in units per 10 mg of tissue.

Measurement of Plasma Cytokines and Chemokines

Serum concentrations of IL-10, IL-6, KC, IL-1β, MIP-1α, TNFα, and LIX were analyzed using a Luminex multiplex system (Luminex Corporation, Austin, TX) according to instructions from the manufacturer.

In Vivo Bacterial Load

Twenty-four hours after CLP mice were sacrificed with carbon dioxide asphyxiation, serum samples were obtained via cardiac puncture and subjected to serial log-fold dilutions using sterile normal saline.105 The dilutions from all samples were then plated onto blood agar plates (Becton Dickinson) and incubated for 24 h in a bacterial culture incubator. After the

24 h incubation period, bacterial culture plates were manually counted by a technician blinded to the experimental conditions.

Supplementary Material

Refer to Web version on PubMed Central for supplementary material.

Acknowledgments

This work was supported by the National Institutes of Health Grants HL07446 (T32 Training Grant, T.R.), DE017139 (B.S.), GM099773 and GM108025 (H.R.W.), and CA098799 (G.B.F.) and a Schrodinger Postdoctoral Fellowship from the Austrian Science Fund (R.F.).

Abbreviations Used

MMP	matrix metalloproteinase
THP	triple-helical peptide
THPI	triple-helical peptide inhibitor
MT1-MMP	membrane type 1 matrix metalloproteinase
Flp	(2*S*,4*R*)-4-fluoroproline
mep	(2*S*,4*R*)-4-methylproline
Fmoc	9-fluorenylmethoxy-carbonyl
MS	multiple sclerosis
BBB	blood–brain barrier
CNS	central nervous system
MOG	myelin oligodendrocyte glycoprotein
EAE	experimental autoimmune encephalomyelitis
TBV	total blood volume
CD	circular dichroism
CLP	cecal ligation and puncture
KC	keratinocyte chemoattractant
LIX	LPS-induced CXC chemokine
MPO	myeloperoxidase
IL	interleukin
MIP	macrophage inflammatory protein
TNF	tumor necrosis factor

Europe PMC Funders Author Manuscripts

TIMP	tissue inhibitor of metal-loproteinase
DMF	*N,N*-dimethylformamide
TFA	trifluoroacetic acid
DCM	dichloromethane
EtOAc	ethyl acetate
NMM	*N*-methylmorpholine
DBU	1,8-diazabicyclo[5.4.0]-undec-7-ene
HCTU	2-(6-chloro-1*H*-benzotriazole-1-yl)-1,1,3,3-tetramethylaminium hexafluorophosphate
Cbz	benzyloxycarbonyl
Bzl	benzyl
EDT	1,2-ethanedithiol
DIPCDI	*N,N*′-diisopropylcarbodiimide
HOBt	1-hydroxybenzotriazole
DIPEA	*N,N*-diisopropylethylamine
AEBSF	4-(2-aminoethyl)-benzensulfonyl fluoride hydrochloride
PBS	phosphate buffered saline
CFA	complete Freund’s adjuvant

References

(1). Song F, Wisithphrom K, Zhou J, Windsor LJ. Matrix metalloproteinase dependent and independent collagen degradation. Front Biosci, Landmark Ed. 2006; 11:3100–3120.

(2). Overall CM, Lopez-Otin C. Strategies for MMP inhibition in cancer: Innovations for the post-trial era. Nat Rev Cancer. 2002; 2:657–672. [PubMed: 12209155]

(3). Egeblad M, Werb Z. New functions for the matrix metalloproteinases in cancer progression. Nat Rev Cancer. 2002; 2:161–174. [PubMed: 11990853]

(4). Fingleton B. Matrix metalloproteinases as valid clinical targets. Curr Pharm Des. 2007; 13:333–346. [PubMed: 17313364]

(5). Fields GB. Interstitial collagen catabolism. J Biol Chem. 2013; 288:8785–8793. [PubMed: 23430258]

(6). Whittaker M, Floyd CD, Brown P, Gearing AJH. Design and therapeutic application of matrix metalloproteinase inhibitors. Chem Rev. 1999; 99:2735–2776. [PubMed: 11749499]

(7). Rao BG. Recent developments in the design of specific matrix metalloproteinase inhibitors aided by structural and computational studies. Curr Pharm Des. 2005; 11:295–322. [PubMed: 15723627]

(8). Hodgson J. Remodeling MMPIs. Bio/Technology. 1995; 13:554–557. [PubMed: 9634794]

(9). Cuniasse P, Devel L, Makaritis A, Beau F, Georgiadis D, Matziari M, Yiotakis A, Dive V. Future challenges facing the development of specific active-site-directed synthetic inhibitors of MMPs. Biochimie. 2005; 87:393–402. [PubMed: 15781327]

(10). Overall CM, Kleifeld O. Towards third generation matrix metalloproteinase inhibitors for cancer therapy. Br J Cancer. 2006; 94:941–946. [PubMed: 16538215]

(11). Vandenbroucke RC, Libert C. Is there new hope for therapeutic matrix metalloproteinase inhibition? Nat Rev Drug Discovery. 2014; 13:904–927. [PubMed: 25376097]

(12). Lauer-Fields JL, Brew K, Whitehead JK, Li S, Hammer RP, Fields GB. Triple-helical transition-state analogs: A new class of selective matrix metalloproteinase inhibitors. J Am Chem Soc. 2007; 129:10408–10417. [PubMed: 17672455]

(13). Georgiadis D, Dive V. Phosphinic peptides as potent inhibitors of zinc-metalloproteases. Top Curr Chem. 2014; 360:1–38.

(14). Lauer-Fields JL, Whitehead JK, Li S, Hammer RP, Brew K, Fields GB. Selective modulation of matrix metalloproteinase 9 (MMP-9) functions via exosite inhibition. J Biol Chem. 2008; 283:20087–20095. [PubMed: 18499673]

(15). Bhowmick M, Stawikowska R, Tokmina-Roszyk D, Fields GB. Matrix metalloproteinase inhibition by heterotrimeric triple-helical peptide transition state analogs. ChemBioChem. 2015; 16:1084–1092. [PubMed: 25766890]

(16). Lauer-Fields JL, Sritharan T, Stack MS, Nagase H, Fields GB. Selective hydrolysis of triple-helical substrates by matrix metalloproteinase-2 and −9. J Biol Chem. 2003; 278:18140–18145. [PubMed: 12642591]

(17). Minond D, Lauer-Fields JL, Cudic M, Overall CM, Pei D, Brew K, Visse R, Nagase H, Fields GB. The roles of substrate thermal stability and P_2 and P_1' subsite identity on matrix metalloproteinase triple-helical peptidase activity and collagen specificity. J Biol Chem. 2006; 281:38302–38313. [PubMed: 17065155]

(18). Dutton G. Development of peptide drugs advances briskly. Gen Eng Biotechnol News. 2007; 27(10)

(19). Thayer AM. Improving peptides. Chem Eng News. 2011 May 30.89:13–20.

(20). Albericio F, Kruger HG. Therapeutic peptides. Future Med Chem. 2012; 4:1527–1531. [PubMed: 22917241]

(21). DePalma A. Peptides: New processes, lower costs. Genet Eng Biotechnol News. 2015; 35(13): 24–26.

(22). Fan C-Y, Huang C-C, Chiu W-C, Lai C-C, Liou G-G, Li H-C, Chou M-Y. Production of multivalent protein binders using a self-trimerizing collagen-like peptide scaffold. FASEB J. 2008; 22:3795–3804. [PubMed: 18635738]

(23). Ndinguri MW, Zheleznyak A, Lauer JL, Anderson CJ, Fields GB. Application of collagen-model triple-helical peptide-amphiphiles for CD44 targeted drug delivery systems. J Drug Delivery. 2012; 2012

(24). Yasui H, Yamazaki CM, Nose H, Awada C, Takao T, Koide T. Potential of collagen-like triple helical peptides as drug carriers: Their In vivo distribution, metabolism, and excretion profiles in rodents. Biopolymers. 2013; 100:705–713. [PubMed: 23494659]

(25). Yamazaki CM, Nakase I, Endo H, Kishimoto S, Mashiyama Y, Masuda R, Futaki S, Koide T. Collagen-like cell-penetrating peptides. Angew Chem, Int Ed. 2013; 52:5497–5500.

(26). Shinde A, Feher KM, Hu C, Slowinska K. Peptide internalization enabled by folding: triple-helical cell-penetrating peptides. J Pept Sci. 2015; 21:77–84. [PubMed: 25524829]

(27). Koide T, Yamamoto N, Taira KB, Yasui H. Fecal excretion of orally administered collagen-like peptides in rats: Contribution of the triple-helical conformation to their stability. Biol Pharm Bull. 2016; 39:135–137. [PubMed: 26725436]

(28). Shoulders MD, Satyshur KA, Forest KT, Raines RT. Stereoelectronic and steric effects in side chains preorganize a protein main chain. Proc Natl Acad Sci U S A. 2010; 107:559–564. [PubMed: 20080719]

(29). Holmgren SK, Bretscher LE, Taylor KM, Raines RT. A hyperstable collagen mimic. Chem Biol. 1999; 6:63–70. [PubMed: 10021421]

(30). Neumann U, Kubota H, Frei K, Ganu V, Leppert D. Characterization of Mca-Lys-Pro-Leu-Gly-Leu-Dpa-Ala-Arg-NH_2, a fluorogenic substrate with increased specificity constants for collagenases and tumor necrosis factor converting enzyme. Anal Biochem. 2004; 328:166–173. [PubMed: 15113693]

(31). Yong VW, Zabad RK, Agrawal S, DaSilva AG, Metz LM. Elevation of matrix metalloproteinases (MMPs) in multiple sclerosis and impact of immunomodulators. J Neurol Sci. 2007; 259:79–84. [PubMed: 17382965]

(32). Javaid MA, Abdallah MN, Ahmed AS, Sheikh Z. Matrix metalloproteinases and their pathological upregulation in multiple sclerosis: an overview. Acta Neurol Belg. 2013; 113:381–390. [PubMed: 24002649]

(33). Pollinger B. IL-17 producing T cells in mouse models of multiple sclerosis and rheumatoid arthritis. J Mol Med. 2012; 90:613–624. [PubMed: 22231742]

(34). Bittner S, Afzali AM, Wiendl H, Meuth SG. Myelin oligodendrocyte glycoprotein (MOG35-55) induced experimental autoimmune encephalomyelitis (EAE) in C57BL/6 mice. J Visualized Exp. 2014 Apr 15.

(35). McCarthy DP, Richards MH, Miller SD. Mouse models of multiple sclerosis: experimental autoimmune encephalomyelitis and Theiler's virus-induced demyelinating disease. Methods Mol Biol. 2012; 900:381–401. [PubMed: 22933080]

(36). Kridel SJ, Sawai H, Ratnikov BI, Chen EI, Li W, Godzik A, Strongin AY, Smith JW. A unique substrate binding mode discriminates membrane type 1-matrix metalloproteinase (MT1-MMP) from other matrix metalloproteinases. J Biol Chem. 2002; 277:23788–23793. [PubMed: 11959855]

(37). Uttamchandani M, Wang J, Li J, Hu M, Sun H, Chen KY-T, Liu K, Yao SQ. Inhibitor fingerprinting of matrix metalloproteases using a combinatorial peptide hydroxamate library. J Am Chem Soc. 2007; 129:7848–7858. [PubMed: 17539636]

(38). Minond D, Lauer-Fields JL, Cudic M, Overall CM, Pei D, Brew K, Moss ML, Fields GB. Differentiation of secreted and membrane-type matrix metalloproteinase activities based on substitutions and interruptions of triple-helical sequences. Biochemistry. 2007; 46:3724–3733. [PubMed: 17338550]

(39). Lauhio A, Hästbacka J, Pettilä V, Tervahartiala T, Karlsson S, Varpula T, Varpula M, Ruokonen E, Sorsa T, Kolho E. Serum MMP-8, -9 and TIMP-1 in sepsis: high serum levels of MMP-8 and TIMP-1 are associated with fatal outcome in a multicentre, prospective cohort study. Hypothetical impact of tetracyclines Pharmacol Res. 2011; 64:590–594. [PubMed: 21742038]

(40). Solan PD, Dunsmore KE, Denenberg AG, Odoms K, Zingarelli B, Wong HR. A novel role for matrix metalloproteinase-8 in sepsis. Crit Care Med. 2012; 40:379–387. [PubMed: 22020238]

(41). Aguirre A, Blázquez-Prieto J, Amado-Rodriguez L, López-Alonso I, Batalla-Solís E, González-López A, Sánchez-Pérez M, Mayoral-Garcia C, Gutiérrez-Fernández A, Albaiceta GM. Matrix metalloproteinase-14 triggers an anti-inflammatory proteolytic cascade in endotoxemia. J Mol Med (Heidelberg, Ger.). 2017; doi: 10.1007/s00109-017-1510-z

(42). Pahwa S, Stawikowski MJ, Fields GB. Monitoring and inhibiting MT1-MMP during cancer initiation and progression. Cancers. 2014; 6:416–435. [PubMed: 24549119]

(43). Devy L, Huang L, Naa L, Yanamandra N, Pieters H, Frans N, Chang E, Tao Q, Vanhove M, Lejeune A, van Gool R, et al. Selective inhibition of matrix metalloproteinase-14 blocks tumor growth, invasion, and angiogenesis. Cancer Res. 2009; 69:1517–1526. [PubMed: 19208838]

(44). Basu B, Correa de Sampaio P, Mohammed H, Fogarasi M, Corrie P, Watkins NA, Smethurst PA, English WR, Ouwehand WH, Murphy G. Inhibition of MT1-MMP activity using functional antibody fragments selected against its hemopexin domain. Int J Biochem Cell Biol. 2012; 44:393–403. [PubMed: 22138224]

(45). Udi Y, Grossman M, Solomonov I, Dym O, Rozenberg H, Moreno V, Cuniasse P, Dive V, Arroyo AG, Sagi I. Inhibition mechanism of membrane metalloprotease by an exosite-swiveling conformational antibody. Structure. 2015; 23:104–115. [PubMed: 25482542]

(46). Sela-Passwell N, Kikkeri R, Dym O, Rozenberg H, Margalit R, Arad-Yellin R, Eisenstein M, Brenner O, Shoham T, Danon T, Shanzer A, et al. Antibodies targeting the catalytic zinc complex

of activated matrix metalloproteinases show therapeutic potential. Nat Med. 2011; 18:143–147. [PubMed: 22198278]

(47). Martens E, Leyssen A, Van Aelst I, Fiten P, Piccard H, Hu J, Descamps FJ, Van den Steen PE, Proost P, Van Damme J, Liuzzi GM, et al. A monoclonal antibody inhibits gelatinase B/MMP-9 by selective binding to part of the catalytic domain and not to the fibronectin or zinc binding domains. Biochim Biophys Acta, Gen Subj. 2007; 1770:178–186.

(48). Marshall DC, Lyman SK, McCauley S, Kovalenko M, Spangler R, Liu C, Lee M, O'Sullivan C, Barry-Hamilton V, Ghermazien H, Mikels-Vigdal A, et al. Selective allosteric inhibition of MMP-9 is efficacious in preclinical models of ulcerative colitis and colorectal cancer. PLoS One. 2015; 10:e0127063. [PubMed: 25961845]

(49). Botkjaer KA, Kwok HF, Terp MG, Karatt-Vellatt A, Santamaria S, McCafferty J, Andreasen PA, Itoh Y, Ditzel HJ, Murphy G. Development of a specific affinity-matured exosite inhibitor to MT1-MMP that efficiently inhibits tumor cell invasion in vitro and metastasis in vivo. Oncotarget. 2016; 7:16773–16792. [PubMed: 26934448]

(50). Gege C, Bao B, Bluhm H, Boer J, Gallagher BM, Korniski B, Powers TS, Steeneck C, Taveras AG, Baragi VM. Discovery and evaluation of a non-Zn chelating, selective matrix metalloproteinase 13 (MMP-13) inhibitor for potential intra-articular treatment of osteoarthritis. J Med Chem. 2012; 55:709–716. [PubMed: 22175799]

(51). Nara H, Sato K, Naito T, Mototani H, Oki H, Yamamoto Y, Kuno H, Santou T, Kanzaki N, Terauchi J, Uchikawa O, et al. Thieno[2,3-d]pyrimidine-2-carboxamides bearing a carboxybenzene group at 5-position: Highly potent, selective, and orally available MMP-13 inhibitors interacting with the S1″ binding site. Bioorg Med Chem. 2014; 22:5487–5505. [PubMed: 25192810]

(52). Nara H, Sato K, Naito T, Mototani H, Oki H, Yamamoto Y, Kuno H, Santou T, Kanzaki N, Terauchi J, Uchikawa O, et al. Discovery of novel, highly potent, and selective quinazoline-2-carboxamide-based matrix metalloproteinase (MMP)-13 inhibitors without a zinc binding group using a structure-based design approach. J Med Chem. 2014; 57:8886–8902. [PubMed: 25264600]

(53). Li JJ, Nahra J, Johnson AR, Bunker A, O'Brien P, Yue W-S, Ortwine DF, Man C-F, Baragi V, Kilgore K, Dyer RD, et al. Quinazolinones and pyrido[3,4-d]pyrimidin-4-ones as orally active and specific matrix metalloproteinase-13 inhibitors for the treatment of osteoarthritis. J Med Chem. 2008; 51:835–841. [PubMed: 18251495]

(54). Blagg JA, Noe MC, Wolf-Gouveia LA, Reiter LA, Laird ER, Chang SP, Danley DE, Downs JT, Elliott NC, Eskra JD, Griffiths RJ, et al. Potent pyrimidinetrione-based inhibitors of MMP-13 with enhanced selectivity over MMP-14. Bioorg Med Chem Lett. 2005; 15:1807–1810. [PubMed: 15780611]

(55). Heim-Riether A, Taylor SJ, Liang S, Gao DA, Xiong Z, August EM, Collins BK, Farmer BT II, Haverty K, Hill-Drzewi M, Junker H-D, et al. Improving potency and selectivity of a new class of non-Zn-chelating MMP-13 inhibitors. Bioorg Med Chem Lett. 2009; 19:5321–5324. [PubMed: 19692239]

(56). Johnson AR, Pavlovsky AG, Ortwine DF, Prior F, Man C-F, Bornemeier DA, Banotai CA, Mueller WT, McConnell P, Yan C, Baragi V, et al. Discovery and characterization of a novel inhibitor of matrix metalloprotease-13 that reduces cartilage damage *in vivo* without joint fibroplasia side effects. J Biol Chem. 2007; 282:27781–27791. [PubMed: 17623656]

(57). Spicer TP, Jiang J, Taylor AB, Choi JY, Hart PJ, Roush WR, Fields GB, Hodder PS, Minond D. Characterization of selective exosite-binding inhibitors of matrix metalloproteinase 13 that prevent articular cartilage degradation in vitro. J Med Chem. 2014; 57:9598–9611. [PubMed: 25330343]

(58). Gao DA, Xiong Z, Heim-Riether A, Amodeo L, August EM, Cao X, Ciccarelli L, Collins BK, Harrington K, Haverty K, Hill-Drzewi M, et al. SAR studies of non-zinc-chelating MMP-13 inhibitors: Improving selectivity and metabolic stability. Bioorg Med Chem Lett. 2010; 20:5039–5043. [PubMed: 20675133]

(59). Piecha D, Weik J, Kheil H, Becher G, Timmermann A, Jaworski A, Burger M, Hofmann MW. Novel selective MMP-13 inhibitors reduce collagen degradation in bovine articular and human osteoarthritis cartilage explants. Inflammation Res. 2010; 59:379–389.

(60). Reiter LA, Freeman-Cook KD, Jones CS, Martinelli GJ, Antipas AS, Berliner MA, Datta K, Downs JT, Eskra JD, Forman MD, Greer EM, et al. Potent, selective pyrimidinetrione-based inhibitors of MMP-13. Bioorg Med Chem Lett. 2006; 16:5822–5826. [PubMed: 16942871]

(61). Engel CK, Pirard B, Schimanski S, Kirsch R, Habermann J, Klingler O, Schlotte V, Weithmann KU, Wendt KU. Structural basis for the highly selective inhibition of MMP-13. Chem Biol. 2005; 12:181–189. [PubMed: 15734645]

(62). Minond D, Lauer-Fields JL, Nagase H, Fields GB. Matrix metalloproteinase triple-helical peptidase activities are differentially regulated by substrate stability. Biochemistry. 2004; 43:11474–11481. [PubMed: 15350133]

(63). Robichaud TK, Steffensen B, Fields GB. Exosite interactions impact matrix metalloproteinase collagen specificities. J Biol Chem. 2011; 286:37535–37542. [PubMed: 21896477]

(64). Lauer JL, Bhowmick M, Tokmina-Roszyk D, Lin Y, Van Doren SR, Fields GB. The role of collagen charge clusters in the regulation of matrix metalloproteinase activity. J Biol Chem. 2014; 289:1981–1992. [PubMed: 24297171]

(65). Gioia M, Monaco S, Fasciglione GF, Coletti A, Modesti A, Marini S, Coletta M. Characterization of the mechanisms by which gelatinase A, neutrophil collagenase, and membrane-type metalloproteinase MMP-14 recognize collagen I and enzymatically process two α-chains. J Mol Biol. 2007; 368:1101–1113. [PubMed: 17379243]

(66). Gentile E, Liuzzi GM. Marine pharmacology: therapeutic targeting of matrix metalloproteinases in neuroinflammation. Drug Discovery Today. 2017; 22:299–313. [PubMed: 27697495]

(67). Gerwien H, Hermann S, Zhang X, Korpos E, Song J, Kopka K, Faust A, Wenning C, Gross CC, Honold L, Melzer N, et al. Imaging matrix metalloproteinase activity in multiple sclerosis as a specific marker of leukocyte penetration of the blood-brain barrier. Sci Transl Med. 2016; 8:364ra152.

(68). Gray E, Thomas TL, Betmouni S, Scolding N, Love S. Elevated matrix metalloproteinase-9 and degradation of perineuronal nets in cerebrocortical multiple sclerosis plaques. J Neuropathol Exp Neurol. 2008; 67:888–899. [PubMed: 18716555]

(69). Romme Christensen J, Börnsen L, Khademi M, Olsson T, Jensen PE, Sørensen PS, Sellebjerg F. CSF inflammation and axonal damage are increased and correlate in progressive multiple sclerosis. Mult Scler. 2013; 19:877–884. [PubMed: 23178691]

(70). Trentini A, Castellazzi M, Cervellati C, Manfrinato MC, Tamborino C, Hanau S, Volta CA, Baldi E, Kostic V, Drulovic J, Granieri E, et al. Interplay between matrix metalloproteinase-9, matrix metalloproteinase-2, and interleukins in multiple sclerosis patients. Dis Markers. 2016; 2016

(71). Rosenberg GA, Kornfeld M, Estrada E, Kelley RO, Liotta LA, Stetler-Stevenson WG. TIMP-2 reduces proteolytic opening of blood-brain barrier by type IV collagenase. Brain Res. 1992; 576:203–207. [PubMed: 1381261]

(72). Rosenberg GA, Dencoff JE, Correa N Jr, Reiners M, Ford CC. Effect of steroids on CSF matrix metalloproteinases in multiple sclerosis: relation to blood-brain barrier injury. Neurology. 1996; 46:1626–1632. [PubMed: 8649561]

(73). Agrawal S, Anderson P, Durbeej M, van Rooijen N, Ivars F, Opdenakker G, Sorokin LM. Dystroglycan is selectively cleaved at the parenchymal basement membrane at sites of leukocyte extravasation in experimental autoimmune encephalomyelitis. J Exp Med. 2006; 203:1007–1019. [PubMed: 16585265]

(74). Dubois B, Masure S, Hurtenbach U, Paemen L, Heremans H, van den Oord J, Sciot R, Meinhardt T, Hämmerling G, Opdenakker G, Arnold B. Resistance of young gelatinase B-deficient mice to experimental autoimmune encephalomyelitis and necrotizing tail lesions. J Clin Invest. 1999; 104:1507–1515. [PubMed: 10587514]

(75). Trentini A, Manfrinato MC, Castellazzi M, Tamborino C, Roversi G, Volta CA, Baldi E, Tola MR, Granieri E, Dallocchio F, Bellini T, et al. TIMP-1 resistant matrix metalloproteinase-9 is the predominant serum active isoform associated with MRI activity in patients with multiple sclerosis. Mult Scler. 2015; 21:1121–1130. [PubMed: 25662349]

(76). Lauer-Fields JL, Chalmers MJ, Busby SA, Minond D, Griffin PR, Fields GB. Identification of specific hemopexin-like domain residues that facilitate matrix metalloproteinase collagenolytic activity. J Biol Chem. 2009; 284:24017–24024. [PubMed: 19574232]

(77). Hu J, Van den Steen PE, Dillen C, Opdenakker G. Targeting neutrophil collagenase/matrix metalloproteinase-8 and gelatinase B/matrix metalloproteinase-9 with a peptidomimetic inhibitor protects against endotoxin shock. Biochem Pharmacol. 2005; 70:535–544. [PubMed: 15992779]

(78). Qiu Z, Zhang F, Gong C, Xu H, Hu J. Fusion Peptides CPU1 and CPU2 Inhibit matrix metalloproteinases and protect mice from endotoxin shock within a strict time window. Inflammation. 2015; 38:2092–2104. [PubMed: 26111477]

(79). Demeestere D, Dejonckheere E, Steeland S, Hulpiau P, Haustraete J, Devoogdt N, Wichert R, Becker-Pauly C, Van Wonterghem E, Dewaele S, Van Imschoot G, et al. Development and validation of a small single-domain antibody that effectively inhibits matrix metalloproteinase 8. Mol Ther. 2016; 24:890–902. [PubMed: 26775809]

(80). Tester AM, Cox JH, Connor AR, Starr AE, Dean RA, Puente XS, López-Otín C, Overall CM. LPS responsiveness and neutrophil chemotaxis in vivo require PMN MMP-8 activity. PLoS One. 2007; 2:e312. [PubMed: 17375198]

(81). Weber GF, Chousterman BG, He S, Fenn AM, Nairz M, Anzai A, Brenner T, Uhle F, Iwamoto Y, Robbins CS, Noiret L, et al. Interleukin-3 amplifies acute inflammation and is a potential therapeutic target in sepsis. Science. 2015; 347:1260–1265. [PubMed: 25766237]

(82). Matter H, Schwab W, Barbier D, Billen G, Haase B, Neises B, Schudok M, Thorwart W, Schreuder H, Brachvogel V, Lönze P, et al. Quantitative structure-activity relationship of human neutrophil collagenase (MMP-8) inhibitors using comparative molecular field analysis and X-ray structure analysis. J Med Chem. 1999; 42:1908–1920. [PubMed: 10354399]

(83). Couper KN, Blount DG, Riley EM. IL-10: The master regulator of immunity to infection. J Immunol. 2008; 180:5771–5777. [PubMed: 18424693]

(84). Urbach C, Gordon NC, Strickland I, Lowne D, Joberty-Candotti C, May R, Herath A, Hijnen D, Thijs JL, Bruijnzeel-Koomen CA, Minter RR, et al. Combinatorial screening identifies novel promiscuous matrix metalloproteinase activities that lead to inhibition of the therapeutic target IL-13. Chem Biol. 2015; 22:1442–1452. [PubMed: 26548614]

(85). Fortelny N, Cox JH, Kappelhoff R, Starr AE, Lange PF, Pavlidis P, Overall CM. Network analyses reveal pervasive functional regulation between proteases in the human protease web. PLoS Biol. 2014; 12:e1001869. [PubMed: 24865846]

(86). Bieth, JG. Leukocyte elastaseHandbook of Proteolytic Enzymes. 2nd ed. Barrett, AJ, Rawlings, ND, Woessner, JF, editors. Elsevier Academic Press; London: 2004. 1517–1523.

(87). Cursio R, Mari B, Louis K, Rostagno P, Saint-Paul M-C, Giudicelli J, Bottero V, Anglard P, Yiotakis A, Dive V, Gugenheim J, et al. Rat liver injury after normothermic ischemia is prevented by a phosphinic matrix metalloproteinase inhibitor. FASEB J. 2002; 16:93–95. [PubMed: 11709491]

(88). Paemen L, Martens E, Masure S, Opdenakker G. Monoclonal antibodies specific for natural human neutrophil gelatinase B used for affinity purification, quantitation by two-site ELISA and inhibition of enzymatic activity. Eur J Biochem. 1995; 234:759–765. [PubMed: 8575432]

(89). Pruijt JF, Fibbe WE, Laterveer L, Pieters RA, Lindley IJ, Paemen L, Masure S, Willemze R, Opdenakker G. Prevention of interleukin-8-induced mobilization of hematopoietic progenitor cells in rhesus monkeys by inhibitory antibodies against the metalloproteinase gelatinase B (MMP-9). Proc Natl Acad Sci U S A. 1999; 96:10863–10868. [PubMed: 10485917]

(90). Hu J, Van den Steen PE, Houde M, Ilenchuk TT, Opdenakker G. Inhibitors of gelatinase B/matrix metalloproteinase-9 activity comparison of a peptidomimetic and polyhistidine with single-chain derivatives of a neutralizing monoclonal antibody. Biochem Pharmacol. 2004; 67:1001–1009. [PubMed: 15104254]

(91). Sandborn WJ, Bhandari BR, Fogel R, Onken J, Yen E, Zhao X, Jiang Z, Ge D, Xin Y, Ye Z, French D, et al. Randomised clinical trial: a phase 1, dose-ranging study of the anti-matrix metalloproteinase-9 monoclonal antibody GS-5745 versus placebo for ulcerative colitis. Aliment Pharmacol Ther. 2016; 44:157–169. [PubMed: 27218676]

(92). Atkinson SJ, Nolan M, Klingbeil L, Harmon K, Lahni P, Zingarelli B, Wong HR. Intestine-derived matrix metalloproteinase-8 is a critical mediator of polymicrobial peritonitis. Crit Care Med. 2016; 44:e200–e206. [PubMed: 26496446]

(93). Atkinson SJ, Varisco BM, Sandquist M, Daly MN, Klingbeil L, Kuethe JW, Midura EF, Harmon K, Opaka A, Lahni P, Piraino G, et al. Matrix metalloproteinase-8 augments bacterial clearance in a juvenile sepsis model. Mol Med. 2016; 22:455–463. [PubMed: 27506554]

(94). Bhowmick M, Sappidi RR, Fields GB, Lepore SD. Efficient synthesis of Fmoc-protected phosphinic pseuedodipeptides: Building blocks for the synthesis of matrix metalloproteinase inhibitors (MMPIs). Biopolymers. 2011; 96:1–3. [PubMed: 20225219]

(95). Bhowmick M, Fields GB. Synthesis of Fmoc-Gly-Ile phosphinic pseudodipeptide: Residue specific conditions for construction of matrix metalloproteinase inhibitor building blocks. Int J Pept Res Ther. 2012; 18:335–339. [PubMed: 24496015]

(96). Bhowmick M, Fields GB. Stabilization of triple-helical peptides for *in vivo* applications. Methods Mol Biol. 2013; 1081:167–194. [PubMed: 24014440]

(97). Del Valle JR, Goodman M. Asymmetric hydrogenations for the synthesis of Boc-protected-4-alkylprolinols and prolines. J Org Chem. 2003; 68:3923–3931. [PubMed: 12737573]

(98). Shoulders MD, Hodges JA, Raines RT. Reciprocity of steric and stereoelectronic effects in the collagen triple helix. J Am Chem Soc. 2006; 128:8112–8113. [PubMed: 16787056]

(99). Stawikowski MJ, Stawikowska R, Fields GB. Collagenolytic matrix metalloproteinase activities towards peptomeric triple-helical substrates. Biochemistry. 2015; 54:3110–3121. [PubMed: 25897652]

(100). Lauer-Fields JL, Cudic M, Wei S, Mari F, Fields GB, Brew K. Engineered sarafotoxins as TIMP-like MMP inhibitors. J Biol Chem. 2007; 282:26948–26955. [PubMed: 17626018]

(101). Copeland, RA. Tight binding inhibitionEvaluation of Enzyme Inhibitors in Drug Discovery. Copeland, RA, editor. John Wiley & Sons, Inc; Hoboken, NJ: 2005. 178–213.

(102). Yiallouros I, Vassiliou S, Yiotakis A, Zwilling R, Stöcker W, Dive V. Phosphinic peptides, the first potent inhibitors of astacin, behave as extremely slow-binding inhibitors. Biochem J. 1998; 331:375–379. [PubMed: 9531473]

(103). Stawikowski, M, Fields, GB. Introduction to peptide synthesisCurrent Protocols in Protein Science. Coligan, JE, Dunn, B, Ploegh, HL, Speicher, DW, Wingfield, PT, editors. John Wiley & Sons, Inc; New York: 2012. 18.1.1–18.1.13.

(104). Solan PD, Piraino G, Hake PW, Denenberg A, O'Connor M, Lentsch A, Zingarelli B. Liver X receptor alpha activation with the synthetic ligand T0901317 reduces lung injury and inflammation after hemorrhage and resuscitation via inhibition of the nuclear factor kappaB pathway. Shock. 2011; 35:367–374. [PubMed: 20926989]

(105). Standage SW, Caldwell CC, Zingarelli B, Wong HR. Reduced peroxisome proliferator-activated receptor alpha expression is associated with decreased survival and increased tissue bacterial load in sepsis. Shock. 2012; 37:164–169. [PubMed: 22089192]

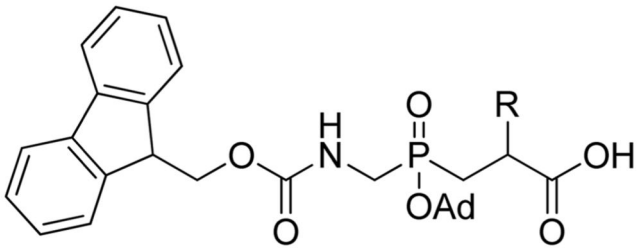

R = Pr^{i} (**3a**); R = Bu^{i} (**3b**)
R = 2-butyl (**3c**)

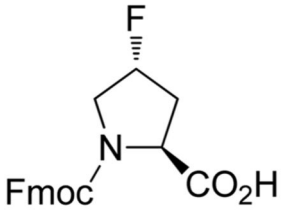

(**4**)

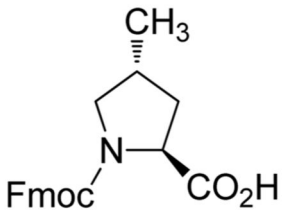

(**5**)

Figure 1.

Structures of Fmoc-phosphinate dipeptide building blocks (**3**), Fmoc-Flp (**4**), and Fmoc-mep (**5**). The phosphinate dipeptides are analogs of Gly-Val (**3a**), Gly-Leu (**3b**), and Gly-Ile (**3c**).

Europe PMC Funders Author Manuscripts

Europe PMC Funders Author Manuscripts

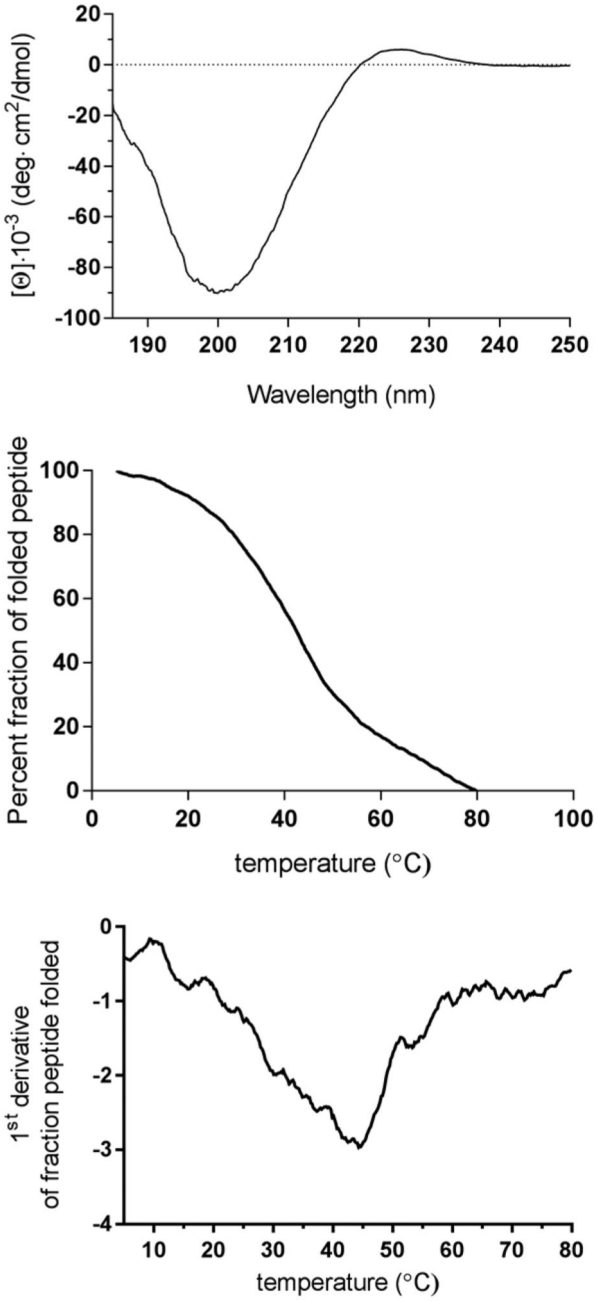

Figure 2.

(Top) CD spectrum of α1(V)GlyΨ{PO_2H-CH_2}Val [$mep_{14,32}$,$Flp_{15,33}$] THPI. (Middle) Thermal transition of α1(V)GlyΨ-{PO_2H-CH_2}Val [$mep_{14,32}$,$Flp_{15,33}$] THPI, measured at λ = 225 nm. (Bottom) First derivative of the thermal transition of α1(V)GlyΨ-{PO_2H-CH_2}Val [$mep_{14,32}$,$Flp_{15,33}$] THPI, indicating T_m = 43.2 °C.

Europe PMC Funders Author Manuscripts

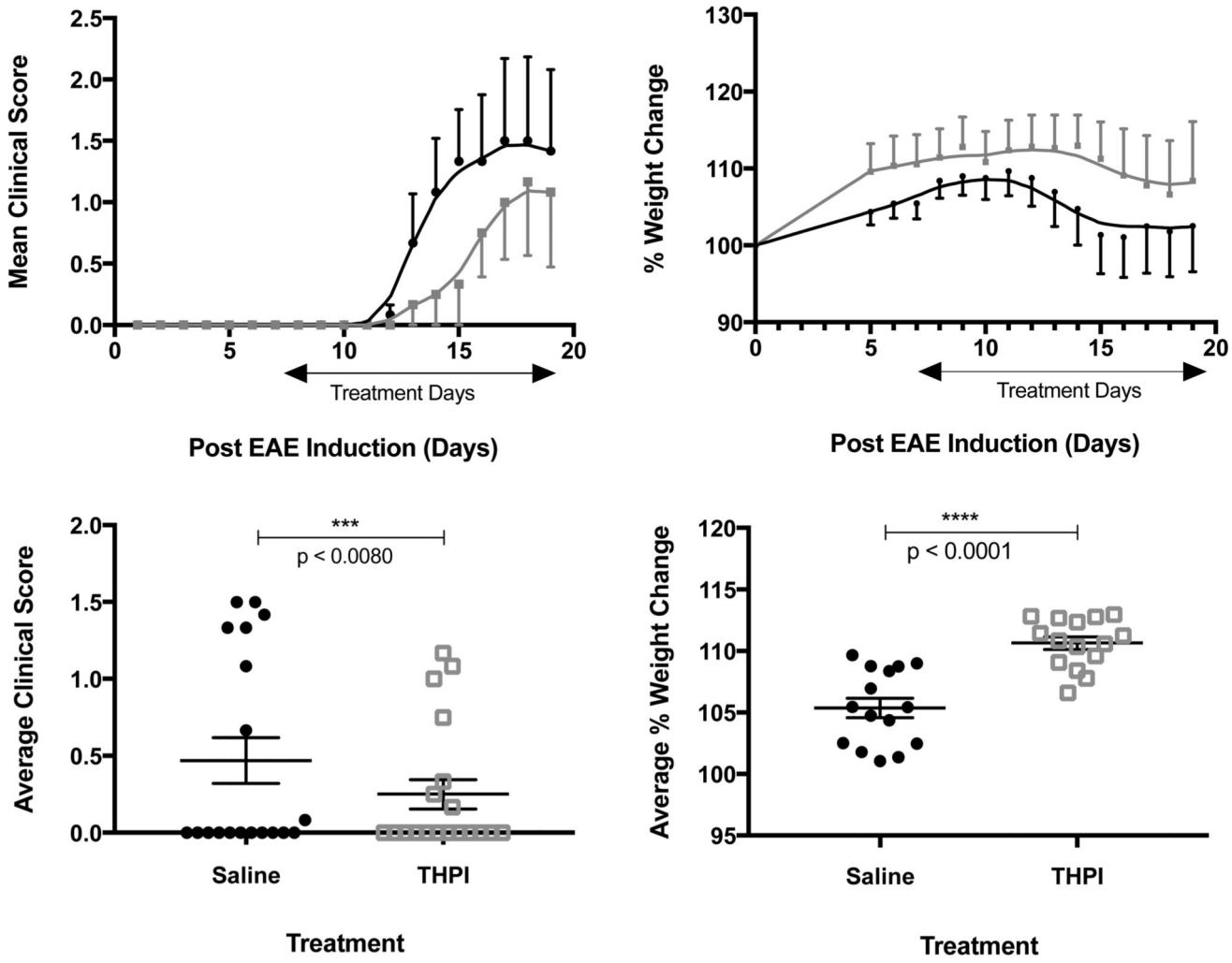

Figure 3.

Results of 12.43 μg of α1(V)GlyΨ{PO_2H-CH_2}Val [$mep_{14,32}$,$Flp_{15,33}$] THPI/day treatment of EAE mice. (A, top left) Clinical score of treated (gray) and nontreated (black) animals. (B, top right) Percent weight change of treated (black) and nontreated (gray) animals. (C, bottom left) Average clinical score of treated and nontreated animals over the course of the experiment. (D, bottom right) Average percent weight change of treated and nontreated animals from induction to sacrifice. $n = 5$ per group, *$p < 0.05$, **$p < 0.01$, ***$p < 0.001$, ****$p < 0.0001$. Statistical analysis was performed using a two-tailed Student t test.

Europe PMC Funders Author Manuscripts

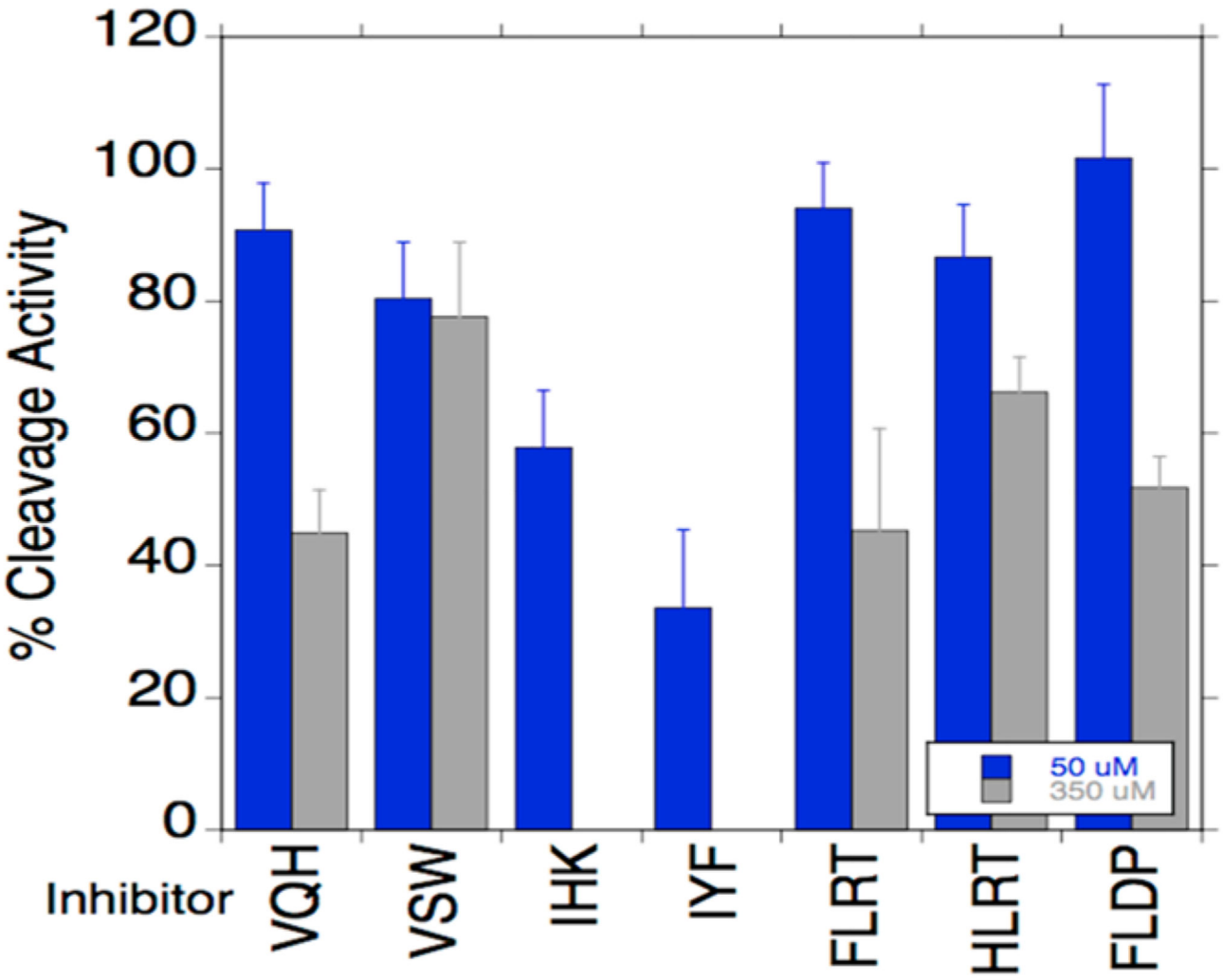

Figure 4.

Inhibition of MT1-MMP hydrolysis of fTHP-15 by THPs. Codes for the THPs are given in the text. THP concentrations were 50 or 350 μM.

Europe PMC Funders Author Manuscripts

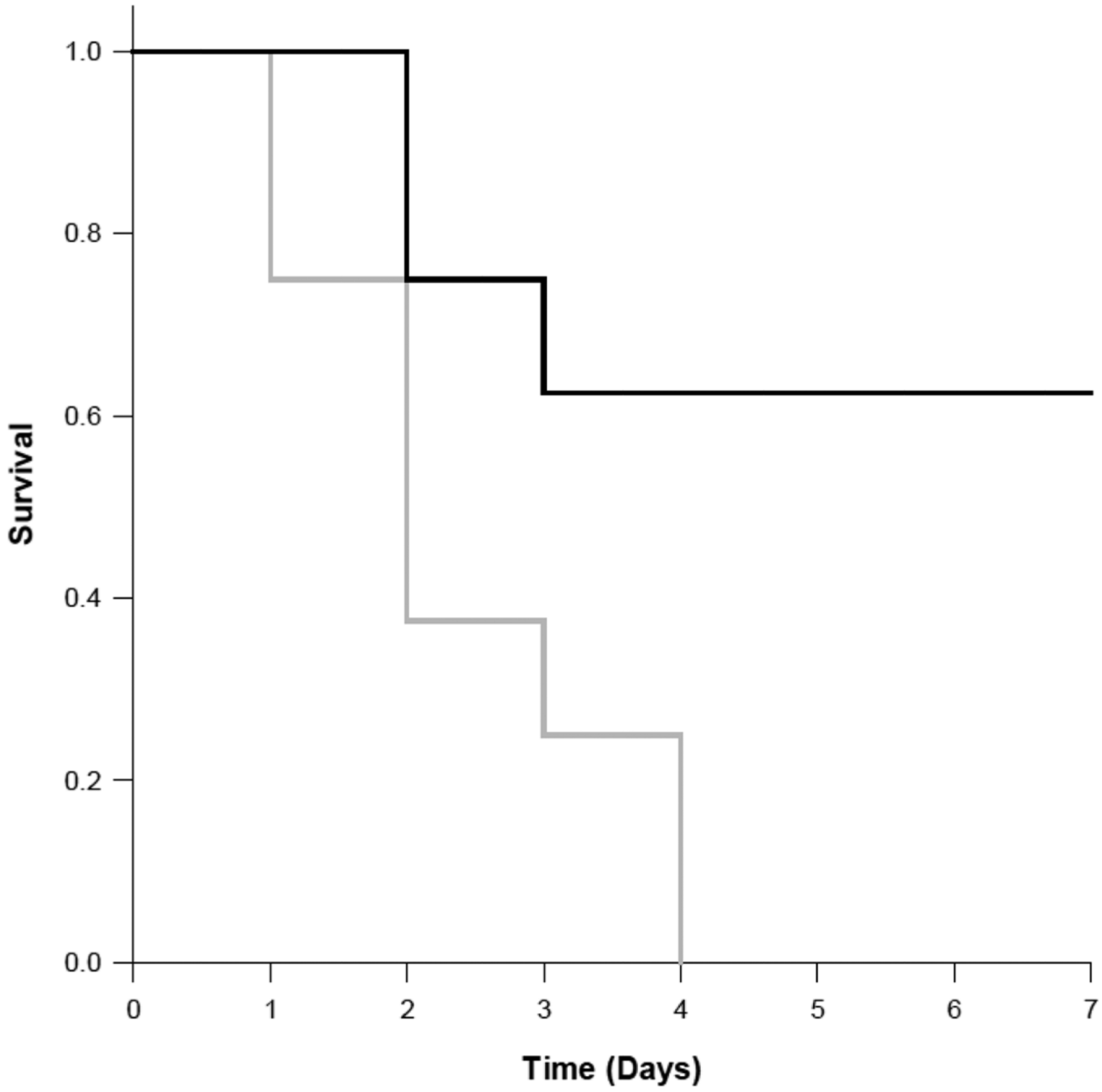

Figure 5.

Seven-day survival curves for wild-type mice subjected to CLP. One group of wild-type mice ($n = 10$) was treated with the GlyΨ{PO_2H-CH_2}Ile-His-Lys-Gln THPI (10 mg/kg) immediately after CLP and then every 12 h for an additional 5 doses (black line). The other group of wild-type mice ($n = 10$) was treated with saline vehicle using the identical schedule (gray line). None of the nontreated wild-type mice survived CLP after 7 days, while 70% of the wild-type mice treated with the THPI survived after 7 days. $p < 0.05$; Kaplan−Meier survival analysis.

Europe PMC Funders Author Manuscripts

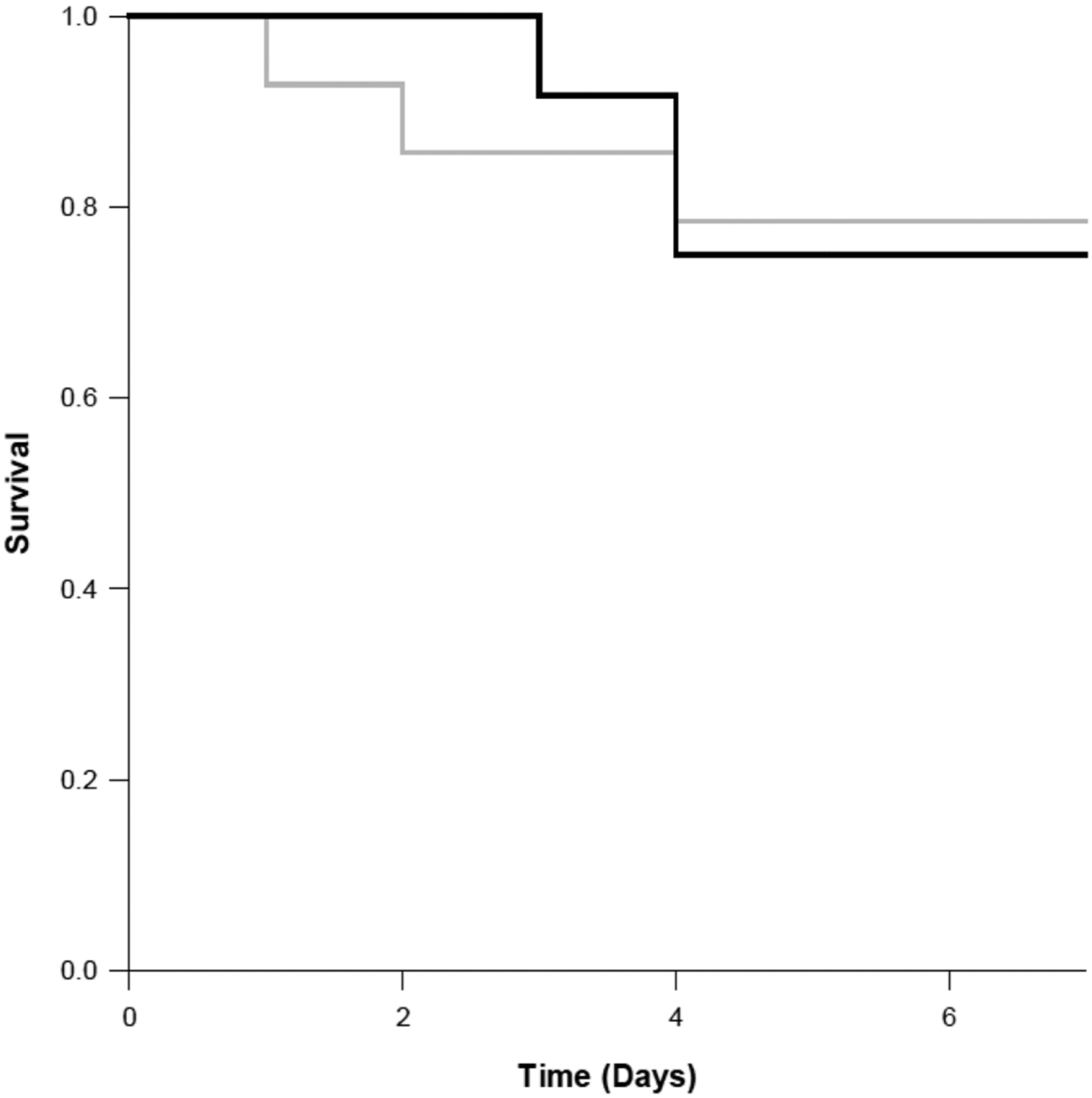

Figure 6.

Seven-day survival curves for Mmp8 null mice subjected to CLP. One group of mice (n = 10) was treated with the GlyΨ{PO_2H-CH_2}Ile-His-Lys-Gln THPI (10 mg/kg) immediately after CLP and then every 12 h for an additional 5 doses (black line). The other group of mice (n = 10) was treated with saline vehicle using the identical schedule (gray line). $p < 0.918$.

Europe PMC Funders Author Manuscripts

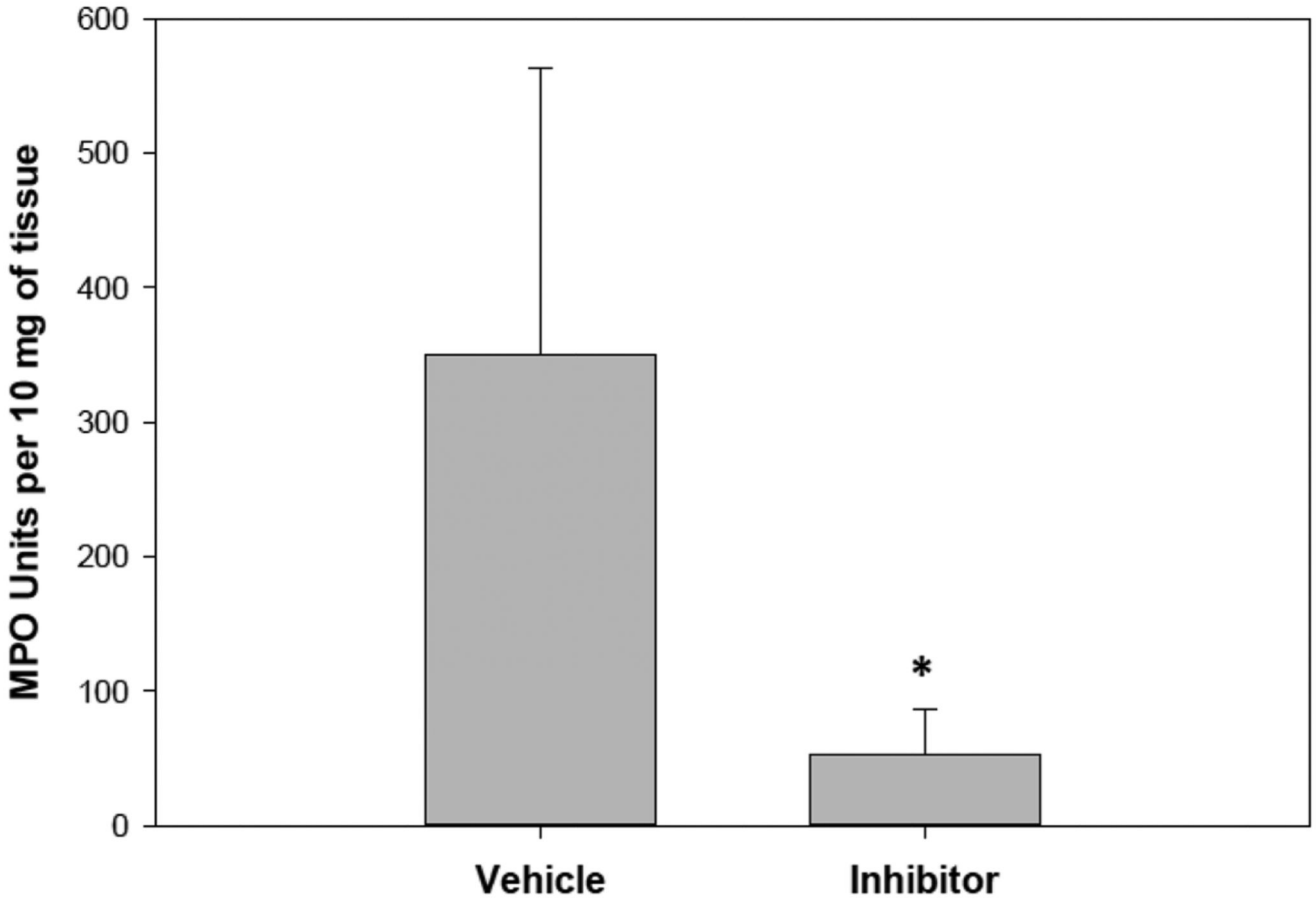

Figure 7.

Wild-type mice lung neutrophil infiltration 24 h after CLP, as measured by MPO activity. One group of wild-type mice ($n = 10$) was treated with the GlyΨ{PO_2H-CH_2}Ile-His-Lys-Gln THPI (10 mg/kg) immediately after CLP and then 12 h later. The other group of wild-type mice ($n = 10$) was treated with saline vehicle using the identical schedule. THPI treatment significantly reduced neutrophil infiltration into the lungs. *$p < 0.05$; Student's t test.

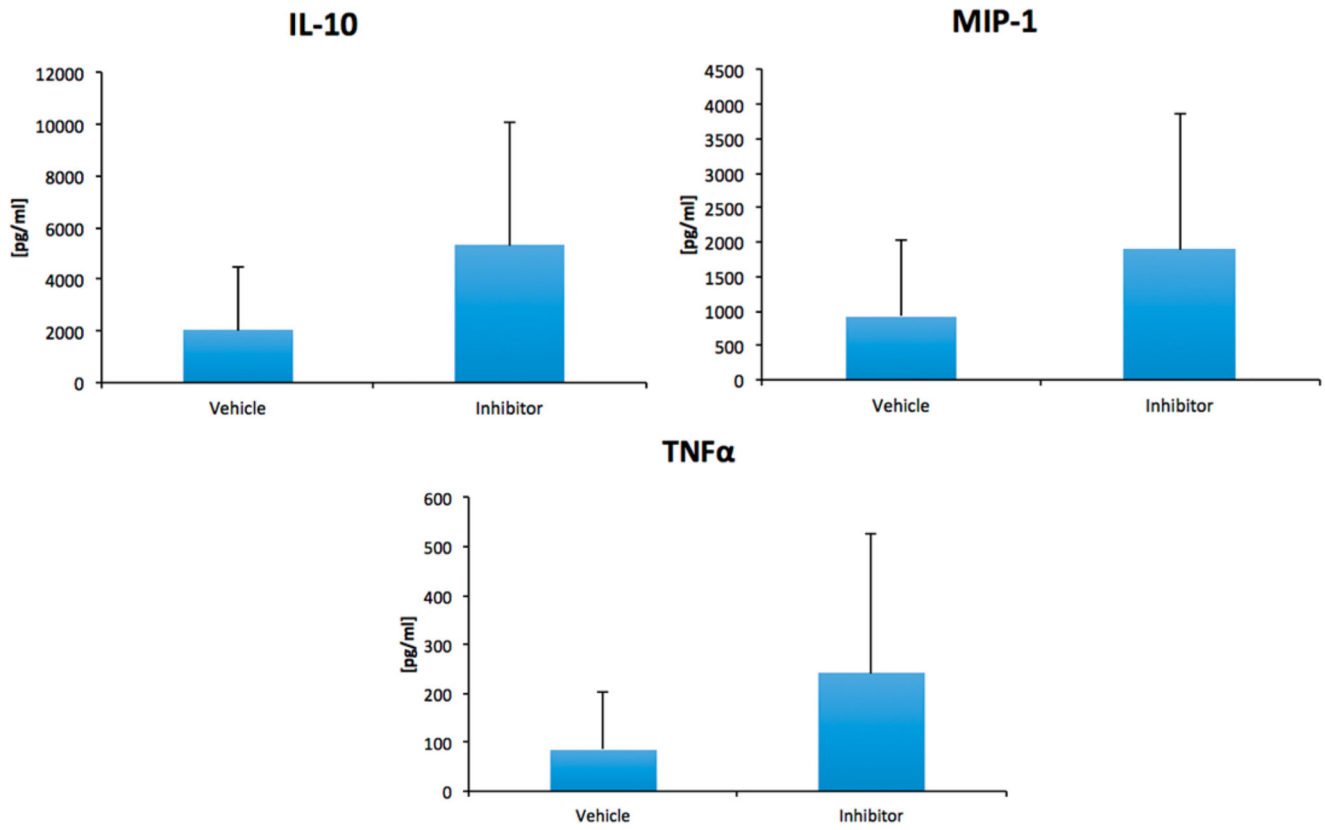

Figure 8.

Wild-type mice serum cytokine profiles 24 h after CLP. One group of mice ($n = 10$) was treated with the GlyΨ{PO_2H-CH_2}Ile-His-Lys-Gln THPI (10 mg/kg) immediately after CLP and then 12 h later. The other group of mice ($n = 10$) was treated with saline vehicle using the identical schedule. $p < 0.05$ versus vehicle.

Europe PMC Funders Author Manuscripts

Table 1

Inhibition of MMP-2 and MMP-9

enzyme	inhibitor	temperature (°C)	$K_i^{(app)}$ (nM)
MMP-2	C_6-α1(V)GlyΨ{PO_2H-CH_2}Val THPI	10	4.14 ± 0.47[a]
MMP-2	C6-α1(V)GlyΨ{PO_2H-CH_2}Val THPI	37	19.23 ± 0.64[a]
MMP-2	α1(V)GlyΨ{PO_2H-CH_2}Val [$mep_{14,32}$,$Flp_{15,33}$] THPI	25	189.1 ± 26.54
	α1(V)GlyΨ{PO_2H-CH_2}Val [$mep_{14,32}$,$Flp_{15,33}$] THPI	37	2.24 ± 0.11
MMP-9	C_6-α1(V)GlyΨ{PO_2H-CH_2}Val THPI	10	1.76 ± 0.05[a]
	C_6-α1(V)GlyΨ{PO_2H-CH_2}Val THPI	37	1.29 ± 0.00[a]
MMP-9	α1(V)GlyΨ{PO_2H-CH_2}Val [$mep_{14,32}$,$Flp_{15,33}$] THPI	25	90.6 ± 6.67
MMP-9	α1(V)GlyΨ{PO_2H-CH_2}Val [$mep_{14,32}$,$Flp_{15,33}$] THPI	37	0.98 ± 0.092

[a]As previously published.12

Europe PMC Funders Author Manuscripts

Table 2

Inhibition of MMPs by GlyΨ{PO_2H-CH_2}Ile THPIs

enzyme	inhibitor	K_i (nM)
MT1-MMP	GlyΨ{PO_2H-CH_2}Ile-His-Lys-Gln THPI	4704 ± 708.4
MMP-8	GlyΨ{PO_2H-CH_2}Ile-His-Lys-Gln THPI	124.6 ± 6.9
MMP-1	GlyΨ{PO_2H-CH_2}Ile-His-Lys-Gln THPI	169.2 ± 28.4
MMP-3	GlyΨ{PO_2H-CH_2}Ile-His-Lys-Gln THPI	NI[a]
MT1-MMP	GlyΨ{PO_2H-CH_2}Ile-Tyr-Phe-Gln THPI	46.15 ± 4.7
MMP-1	GlyΨ{PO_2H-CH_2}Ile-Tyr-Phe-Gln THPI	110.59 ± 29.8
MMP-2	GlyΨ{PO_2H-CH_2}Ile-Tyr-Phe-Gln THPI	17.82 ± 1.9
MMP-3	GlyΨ{PO_2H-CH_2}Ile-Tyr-Phe-Gln THPI	13600.33 ± 5160.7
MMP-8	GlyΨ{PO_2H-CH_2}Ile-Tyr-Phe-Gln THPI	62.1 ± 2.5
MMP-9	GlyΨ{PO_2H-CH_2}Ile-Tyr-Phe-Gln THPI	0.03 ± 0.02
MMP-13		77.13 ± 14.4

[a]NI = no inhibition at a THPI concentration of 1000 nM.